On a fully-implicit VMS-stabilized FE formulation for low Mach number compressible resistive MHD with application to MCF

Bonilla de Toro, Jesus
Shadid, John N.
Tang, Xianzhu
Crockatt, Michael M.
Ohm, Peter
Phillips, E.
Pawlowski, R. P.
Conde, S.
Beznosov, Oleksii

To be published in: Computer Methods in Applied Mechanics and Engineering

DOI to publisher's version: 10.1016/j.cma.2023.116359

Available online at www.sciencedirect.com
ScienceDirect
Comput. Methods Appl. Mech. Engrg. xxx (xxxx) xxx
Computer methods in applied mechanics and engineering
www.elsevier.com/locate/cma

On a fully-implicit VMS-stabilized FE formulation for low Mach number compressible resistive MHD with application to MCF☆

J. Bonilla[a,*], J.N. Shadid[b,c], X.-Z. Tang[a], M.M. Crockatt[b], P. Ohm[d], E.G. Phillips[b,1], R.P. Pawlowski[b], S. Conde[b,2], O. Beznosov[a]

[a] *Los Alamos National Laboratory, Los Alamos, NM, United States of America*
[b] *Sandia National Laboratories, Albuquerque, NM, United States of America*
[c] *University of New Mexico, Albuquerque, NM, United States of America*
[d] *RIKEN Center for Computational Science, Japan*

Available online xxxx

Abstract

This study presents the development and evaluation of a fully-implicit variational multiscale (VMS) stabilized unstructured finite element (FE) formulation for compressible magnetohydrodynamics (MHD) model, at low Mach number regime. The model describes the dynamics of a compressible conducting fluid in the low Mach number limit in the presence of electromagnetic fields and can be used to study aspects of astrophysical phenomena, important science and technology applications, and basic plasma physics phenomena. The specific applications that motivate this study are macroscopic simulations of the longer time-scale stability and disruptions of magnetic confinement fusion (MCF) devices, specifically the ITER tokamak. The discussion considers the development of the VMS FE representation, the structure of the stabilizing terms that deal with significant convective flows, the stabilization of the nearly incompressible response of the fluid flow, and the stabilization of the constraint that enforces the solenoidal involution on the magnetic field. The nonlinear discretized system is solved with scalable preconditioned Newton–Krylov iterative methods, which employs a multiphysics block preconditioning method based on approximate block factorizations and Schur complements. The study presents an evaluation of the VMS method on a 2D cartesian tearing mode instability, and illustrates the scalability of the solvers on MCF relevant problems. A set of results are also presented for longer time-scale stability and disruptions for the ITER tokamak. These include a vertical displacement event (VDE), and a (1,1) internal kink mode. The formulation is demonstrated to be scalable and also reasonably robust with respect to the Lundquist number scaling.

Keywords: Compressible resistive MHD; VMS FE; Tokamak VDE; Fully-implicit Newton–Krylov; Block preconditioning; AMG

☆ This work was partially supported by the U.S. Department of Energy (DOE), Office of Science, Office of Advanced Scientific Computing Research, Applied Mathematics Program, by the U.S. Department of Energy, Office of Science, Office of Advanced Scientific Computing Research and Office of Fusion Energy Sciences, Scientific Discovery through the Advanced Computing (SciDAC) program under the Tokamak Disruption Simulation project.This research used resources provided by the Los Alamos National Laboratory Institutional Computing Program, which is supported by the U.S. Department of Energy National Nuclear Security Administration under Contract No. 89233218CNA000001..
* Corresponding author.
E-mail addresses: jbonilla@lanl.gov (J. Bonilla), jnshadi@sandia.gov (J.N. Shadid), xtang@lanl.gov (X.-Z. Tang), mmcrock@sandia.gov (M.M. Crockatt), peter.ohm@riken.jp (P. Ohm), egphill@sandia.gov (E.G. Phillips), rppawlo@sandia.gov (R.P. Pawlowski), sconde89@gmail.com (S. Conde), obeznosov@lanl.gov (O. Beznosov).
[1] Contractor.
[2] Collaborator.

https://doi.org/10.1016/j.cma.2023.116359
0045-7825/

Please cite this article as: J. Bonilla, J.N. Shadid, X.-Z. Tang et al., On a fully-implicit VMS-stabilized FE formulation for low Mach number compressible resistive MHD with application to MCF, Computer Methods in Applied Mechanics and Engineering (2023) 116359, https://doi.org/10.1016/j.cma.2023.116359.

1. Introduction

Fluid models of plasma can be useful computational analysis tools for the study of macroscopic behavior of plasma flows in a broad range of scientific and engineering applications. These models describe the dynamics of a compressible conducting fluid in presence of electromagnetic fields, which can be used to study aspects of astrophysical phenomena, basic plasma physical phenomena, and science and technology applications. The governing partial differential equations (PDEs) for a base-level continuum MHD model consist of conservation of mass, momentum and energy augmented by the low-frequency Maxwell's equations. This system of PDEs is non-self adjoint, strongly coupled, highly nonlinear, and is characterized by multiple physical mechanisms that span a large range of length- and time-scales [1]. These characteristics make the scalable, robust, accurate, and efficient computational solution of these systems extremely challenging at long time-scales. From this point of view, fully-implicit formulations, coupled with effective robust nonlinear iterative solution methods –in this study Newton–Krylov methods– become attractive, as they have the potential to provide stable, higher-order time integration of these complex multiphysics systems for longer time-scale simulations. These methods can follow the dynamical time-scales of interest, as opposed to time-scales determined by either numerical stability or by temporal order-of-accuracy reduction [2–6].

The specific science and technology applications that motivates this study are longer time-scale macroscopic stability and disruption of magnetic confinement fusion (MCF) devices, specifically the ITER tokamak [7,8]. Tokamak devices are a type of magnetic confinement fusion reactor that use strong magnetic fields to confine a very high temperature plasma ($\approx 100M$ K) of deuterium and tritium to create conditions necessary for nuclear fusion to occur. Of particular interest in this study is the long time scale macroscopic dynamics of these types of devices. Performing these types of simulations can be an important design and operational tool to ensure efficient operation of MCF devices, such as ITER [7,9]. Some plasma instabilities can lead to disruptions in MCF devices. A disruption is a sudden loss of plasma confinement, which can deposit huge thermal energy loads on the walls, as well as induce very large currents and forces in the structure. Understanding the evolution, control (or at least mitigation) of disruptions in ITER is a concern [10,11], since it might only be able to sustain a few major disruptions before needing shutdown for long maintenance cycles [12].

This paper presents an initial implicit variational multiscale (VMS) stabilized unstructured finite element (FE) formulation for the low Mach number regime of compressible visco-resistive magnetohydrodynamics (MHD). The proposed formulation extends the formulation in [5] to compressible flows and MCF type applications. Several stabilized formulations have been published to date for incompressible MHD flows [4,5,13–17], and for [9] for compressible MHD. This study focuses on the special case of low Mach number regime, where special treatment to the VMS terms in the density equation is required to control the arising saddle point behavior when $\nabla \cdot \mathbf{u} \approx 0$. However, the model still considers ideal gas law equation of state to compute the pressure, i.e, no low Mach number asymptotic limit PDE formulation has been considered for the flow problem. An additional benefit of our VMS FE spatial discretization is that this is a fully 3D finite element approximation that does not assume any toroidal symmetry in the formulation as is common in a number of MCF codes [18,19].

The divergence-free constraint on the magnetic field is enforced using a Lagrange multiplier [13]. This has been successfully used for various stabilized and mixed FE incompressible MHD formulations (see references in [17, Table 1] and in [5]). This formulation enforces the divergence-free condition weakly and induces an elliptic type constraint. This constraint introduces a saddle point type problem structure that requires appropriate VMS type formulation [4,5,13–17]. An additional complexity is that the low Mach number flow and the presence of a large-magnetic field [20–22] produces a nearly incompressible flow response of the system for which we structure the VMS stabilization to handle this saddle point system as well as upwinding the continuity equation following some similar ideas in the arbitrary Lagrangian Eulerian (ALE) context in the work [23,24] for compressible flows.

To evaluate the effectiveness of the proposed VMS formulation numerical test have been performed to demonstrate the improved behavior of the scheme for the low Mach number regime. Moreover, a 2D Cartesian tearing mode problem is used to compare the mode growth rates against results from the literature. Then a series of 3D results using the ITER geometry are pursued to show the effectiveness of the presented method for the simulation of longer time-scale instabilities. In particular, a vertical displacement event (VDE) and a (1,1) internal kink mode are presented. Finally, an overview of the algorithmic strong scalability is presented, along with scaling robustness with respect to the Lundquist number.

The paper is structured as follows: Section 2 introduces the model equations in strong and its variational weak forms; Section 3 contains the main result of this work, the finite element discretization of the problem using a VMS approach to stabilize it; in Section 4 an overview of the time integration and the preconditioning strategy is given; finally, in Section 5 the practicality of the formulation is demonstrated with a series of numerical results, and some conclusions are drawn in Section 6.

2. Compressible visco-resistive MHD equations

In the present study we consider the single fluid compressible visco-resistive MHD system of equations. This system consists of the mass, momentum, and internal energy balance laws coupled with an induction form for the reduced Maxwell's equations [5], and is given by

$$\frac{\partial \rho}{\partial t} + \nabla \cdot (\rho \mathbf{u}) = 0, \tag{1a}$$

$$\frac{\partial (\rho \mathbf{u})}{\partial t} + \nabla \cdot [(\rho \mathbf{u} \otimes \mathbf{u}) + pI + \boldsymbol{\pi}] - \mathbf{j} \times \mathbf{B} = \mathbf{0}, \tag{1b}$$

$$\frac{n}{\gamma - 1}\frac{\partial T}{\partial t} + \frac{n}{\gamma - 1}\mathbf{u} \cdot \nabla T + p(\nabla \cdot \mathbf{u}) + \nabla \cdot \mathbf{q} - \eta \|\mathbf{j}\|^2 - \boldsymbol{\pi} : \nabla \mathbf{u} = 0, \tag{1c}$$

$$\frac{\partial \mathbf{B}}{\partial t} + \nabla \cdot \left[\mathbf{u} \otimes \mathbf{B} - \mathbf{B} \otimes \mathbf{u} - \frac{\eta}{\mu_0}(\nabla \mathbf{B} - (\nabla \mathbf{B})^T) \right] = \mathbf{0}, \tag{1d}$$

$$\nabla \cdot \mathbf{B} = 0, \tag{1e}$$

where unknowns are density, ρ, momentum, $\mathbf{m} = \rho \mathbf{u}$, magnetic field, $\mathbf{B}$, and temperature, T (given in energy units, i.e., $T = T' k_b$ where k_b is the Boltzmann's constant). p is the pressure, and the number density, n, is computed as $n = \rho / m_i$, where m_i is the ion mass. The fluid viscosity tensor is denoted as $\boldsymbol{\pi}$, and $\mathbf{q}$ is the heat flux, and I is a 3 by 3 identity matrix. The ideal gas equation of state in this scaling for temperature is, $p = nT$, and Ampère's law for the plasma current, $\mathbf{j} = \mu_0^{-1} \nabla \times \mathbf{B}$, close the system. The physical parameters η, γ, correspond to the electrical resistivity, and the adiabatic index, respectively.

In a hot magnetized plasma –when the thermal and fluid velocities are comparable–, the momentum flux is temperature dependent and substantially different in each direction. This leads to a complex viscous tensor structure, see [25, Ch. 4.6]. However, the viscous terms are small in comparison with the rest of the terms in the momentum equation [25, pag. 82]. Therefore, for the sake of simplicity, in the present work the Navier–Stokes viscous tensor for a monoatomic gas is considered, which reads

$$\boldsymbol{\pi} = \frac{2}{3}\mu(\nabla \cdot \mathbf{u})I - \mu(\nabla \mathbf{u} + (\nabla \mathbf{u})^T),$$

where μ is the dynamic viscosity.

Similarly, the heat flux is also temperature-dependent and anisotropic. Even though a simplified definition with a constant isotropic conductivity might be used for simplified examples, the anisotropic behavior $\mathbf{q}$ cannot be neglected for the current problems of interest. Thus, for a single-fluid formulation, the heat flux takes the form

$$\mathbf{q} \doteq -\kappa_{||} \nabla_{||} T - \kappa_{\perp} \nabla_{\perp} T,$$

where $\kappa_{||}$, $\kappa_{\perp}$, are the heat conductivities in each direction and the directional gradients are defined as

$$\nabla_{||}(\cdot) \doteq (\mathbf{b} \cdot \nabla(\cdot))\mathbf{b}, \quad \text{and} \quad \nabla_{\perp}(\cdot) \doteq \nabla(\cdot) - \nabla_{||}(\cdot),$$

where $\mathbf{b}$ is the unit vector pointing the direction of $\mathbf{B}$, $\mathbf{b} \doteq \mathbf{B}/\|\mathbf{B}\|$. Notice that the isotropic Fourier heat flux, $\mathbf{q} \doteq -\kappa \nabla T$, can be recovered for $\kappa_{||} = \kappa_{\perp}$. Closed expressions for two-fluid description of the plasma flow can be found in Braginskii's review [26]. Since the heat flow phenomenon is dominated by the electrons, i.e., the parallel heat conductivity for electrons, $\kappa_{||}^e$, and the parallel heat conductivity for ions, $\kappa_{||}^i$, are related $\kappa_{||}^e / \kappa_{||}^i \approx 49$; the expressions for the electron conductivities are used for the single fluid descriptions. Thus, the thermal conductivities read

$$\kappa_{||} \doteq 3.16 \frac{nT\tau_e}{m_e} \quad \kappa_{\perp} \doteq 4.66 \frac{nT}{m_e \Omega_e^2 \tau_e}.$$

The conductivities depend on the electron cyclotron frequency, $\Omega_e = -eB/m_e$, and the electron collision time

$$\tau_e = \frac{6\pi\sqrt{2\pi m_e}\ \varepsilon_0^2\ T^{3/2}}{\lambda n e^4},$$

where, e is the electron charge, m_e is the electron mass, ε_0 is the vacuum permittivity, and λ is the Coulomb logarithm.

The resistivity, η, is also anisotropic and temperature-dependent in hot magnetized plasmas. In contrast to the thermal conductivities, the anisotropy ratio in this case is $\eta_{||}/\eta_{\perp} \sim 0.51$. Hence, using an isotropic value is still considered a reasonable approximation. Spitzer's model provides a temperature dependent resistivity that reads

$$\eta = \frac{m_e}{e^2 n \tau_e}.$$

The resistive MHD model exhibits the involution $\nabla \cdot B = 0$. There exist several techniques to enforce this magnetic solenoidal constraint [5,17,27]. In this formulation, a scalar Lagrange multiplier, ψ, is introduced in the induction equation to the allow enforcement of the involution as a constraint. This technique is well known and has been successfully used in the context of finite elements [5,13–15] and finite volumes [27,28]. In this case the modified induction equation is

$$\frac{\partial \mathbf{B}}{\partial t} + \nabla \cdot \left[\mathbf{u} \otimes \mathbf{B} - \mathbf{B} \otimes \mathbf{u} - \frac{\eta}{\mu_0}(\nabla \mathbf{B} - (\nabla \mathbf{B})^T) + \psi I \right] = \mathbf{0}, \tag{2}$$

and then it is possible to explicitly enforce the constraint $\nabla \cdot \mathbf{B} = 0$ in the system of balance equations.

2.1. Dimensionless form

The governing balance law system is made dimensionless using the following common definitions, which are often referred as Alfvènic units [29]. This transformation scales the unknowns, that can differ by several orders of magnitude, to have similar magnitudes. In particular, the set of dimensionless unknowns and parameters are

$$\begin{aligned}
&t \to t_0 \tilde{t}, && \boldsymbol{x} \to L_0 \tilde{\mathbf{x}}, && \mathbf{B} \to B_0 \tilde{\mathbf{B}}, && T \to T_0 \tilde{T},\\
&\rho \to \rho_0 \tilde{\rho}, && \psi \to \psi_0 \tilde{\psi}, && \nabla \to \tfrac{1}{L_0}\tilde{\nabla}, && p \to p_0 \tilde{p},\\
&\mathbf{u} \to u_0 \tilde{\mathbf{u}}, && \mathbf{E} \to E_0 \tilde{\mathbf{E}}, && \mathbf{j} \to j_0 \tilde{\mathbf{j}}, && n \to n_0 \tilde{n} = \tfrac{\rho_0}{m_i}\tilde{n}.
\end{aligned}$$

where the following relations hold

$$u_0 = \tfrac{L_0}{t_0}, \qquad u_0 = u_A = \tfrac{B_0}{\sqrt{\mu_0 \rho_0}}, \qquad E_0 = u_0 B_0, \qquad j_0 = \tfrac{B_0}{\mu_0 L_0}, \qquad \tilde{\rho} = \tilde{n},$$

with the definition of the Alfvèn velocity, u_A. After substitution of the above relations into (1)–(2), and rearranging terms we obtain the following dimensionless system

$$\frac{\partial \tilde{\rho}}{\partial \tilde{t}} + \tilde{\nabla} \cdot (\tilde{\rho}\tilde{\mathbf{u}}) = 0, \tag{3a}$$

$$\frac{\partial (\tilde{\rho}\tilde{\mathbf{u}})}{\partial \tilde{t}} + \tilde{\nabla} \cdot \left[(\tilde{\rho}\tilde{\mathbf{u}} \otimes \tilde{\mathbf{u}}) + \frac{1}{2}\beta \tilde{p} I + \frac{2}{3}\frac{1}{Re}(\tilde{\nabla} \cdot \tilde{\mathbf{u}}) I - \frac{1}{Re}(\tilde{\nabla}\tilde{\mathbf{u}} + (\tilde{\nabla}\tilde{\mathbf{u}})^T) \right] - \tilde{\mathbf{j}} \times \tilde{\mathbf{B}} = \mathbf{0}, \tag{3b}$$

$$\frac{\tilde{n}}{\overline{\gamma}}\frac{\partial \tilde{T}}{\partial \tilde{t}} + \frac{\tilde{n}}{\overline{\gamma}}\tilde{\mathbf{u}} \cdot \tilde{\nabla}\tilde{T} + \tilde{n}\tilde{T}(\tilde{\nabla} \cdot \tilde{\mathbf{u}}) + \tilde{\nabla} \cdot \tilde{\mathbf{q}} - \frac{2}{\beta S}\|\tilde{\mathbf{j}}\|^2 - \frac{\mu}{t_0 p_0}\tilde{\boldsymbol{\pi}} : \tilde{\nabla}\tilde{\mathbf{u}} = 0, \tag{3c}$$

$$\frac{\partial \tilde{\mathbf{B}}}{\partial \tilde{t}} + \tilde{\nabla} \cdot \left[\tilde{\mathbf{u}} \otimes \tilde{\mathbf{B}} - \tilde{\mathbf{B}} \otimes \tilde{\mathbf{u}} - \frac{1}{S}(\tilde{\nabla}\tilde{\mathbf{B}} - (\tilde{\nabla}\tilde{\mathbf{B}})^T) + \frac{\psi_0}{B_0 u_0}\tilde{\psi} I \right] = \mathbf{0}, \tag{3d}$$

$$\tilde{\nabla} \cdot \tilde{\mathbf{B}} = 0, \tag{3e}$$

where

$$\beta = \frac{p_0}{\frac{B_0^2}{2\mu_0}}, \quad Re = \frac{L_0 \rho_0 u_0}{\mu}, \quad \overline{\gamma} = \gamma - 1, \quad \text{and} \quad S = \frac{\mu_0 L_0 u_0}{\eta}$$

are the plasma beta parameter that is a ratio of the plasma fluid pressure to the magnetic field isotropic pressure, the Reynolds number, the adiabatic index minus one, and the Lundquist number. Since we have set the characteristic

velocity equal to the Alfvén speed, the Lundquist number is also equal to the coupling number or Stuart number. Notice the Alfvén speed has been used in the definition of the Reynolds number instead of the standard characteristic fluid velocity. The heat flux becomes

$$\tilde{\mathbf{q}} = -\kappa_{0,||}\tilde{\kappa}_{||}\tilde{\nabla}_{||}\tilde{T} - \kappa_{0,\perp}\tilde{\kappa}_{\perp}\tilde{\nabla}_{\perp}\tilde{T},$$

with

$$\kappa_{0,||} = 3.16\frac{T_0\tau_{0,e}}{L_0u_0m_e}, \quad \text{and} \quad \kappa_{0,\perp} = 4.66\frac{T_0}{L_0u_0m_e\Omega_{0,e}^2\tau_{0,e}},$$

where

$$\tau_{0,e} = \frac{6\pi\sqrt{2\pi m_e}T_0^{3/2}}{\lambda_0 e^4}, \quad \Omega_{0,e} = -\frac{eB_0}{m_e},$$

and

$$\tilde{\kappa}_{||} = \frac{\tilde{T}^{5/2}}{\tilde{\lambda}\tilde{n}}, \text{ and } \quad \tilde{\kappa}_{\perp} = \frac{\tilde{n}\tilde{\lambda}}{\tilde{B}^2\tilde{T}^{1/2}},$$

These dimensionless parameters have the following interpretation in the context of time-scales. Namely, the transport time scale, $\tau_A = L_0/u_A$, the viscous time scale, $\tau_{\mathbf{m}u} = L_0^2\rho_0/\mu$, the resistive time scale, $\tau_\eta = L_0^2\mu_0/\eta$, and the thermal diffusion time scales $\tau_{\kappa_{||}} = L_0^2m_e/3.16T_0\tau_{0,e}$, $\tau_{\kappa_\perp} = L_0^2m_e\Omega_{0,e}^2\tau_{0,e}/4.66T_0$,

$$Re = \frac{\tau_{\mathbf{m}}u}{\tau_A} =: \tilde{\mu}^{-1}, \quad S = \frac{\tau_\eta}{\tau_A} =: \tilde{\eta}^{-1}, \quad Pr_m = \frac{\tau_\eta}{\tau_\mu}, \quad \kappa_{0,||}^{-1} = \frac{\tau_{\kappa_{||}}}{\tau_A}, \quad \kappa_{0,\perp}^{-1} = \frac{\tau_{\kappa_\perp}}{\tau_A}.$$

The definitions of Lundquist, Reynolds, and magnetic Prandtl number then imply $Re = Pr_mS$. The reminder of the parameters L_0, B_0, ρ_0, p_0, T_0 are chosen such that the solution unknown magnitudes are close to unity. Notice that if one chooses $p_0 = \rho_0u_A^2$ the $\frac{1}{2}\beta$ factor becomes equal to one, and $\frac{\mu}{t_0p_0} = Re^{-1}$ in Eqs. (3). However, the dimensionless pressure might not be of the order of unity. Similarly, $\psi_0 = B_0u_0$ is chosen for the sake of simplicity. In subsequent sections, all tildes are dropped for convenience of notation.

Employing directly the definitions of $\kappa_{0,||}$, and $\kappa_{0,\perp}$, above for actual fusion plasma temperatures leads to very large anisotropy ratios for the heat conductivity, and for the magnitude of the Lundquist number [30]. Commonly, in numerical computations a reduction in the range of these variables is applied, e.g., [31–34]. Therefore, in this initial study these conditions are relaxed and for the examples we state the values that are used for $\kappa_{0,||}$, and $\kappa_{0,\perp}$ and the Lundquist number, S.

2.2. Variational weak form

The following standard notation is used for development of the weak form. Consider an open, bounded domain $\Omega \subset \mathbb{R}^d$, where d is the number of spatial dimensions. Let $\partial\Omega$ be the boundary of Ω, we define Γ_D^α as the portion of $\partial\Omega$ where Dirichlet boundary conditions are imposed for the unknown α. Similarly, $\Gamma_N^\alpha = \partial\Omega\backslash\Gamma_D^\alpha$ denotes the portion of $\partial\Omega$ where Neumann boundary conditions are imposed for the unknown α. We denote by $L^2(\Omega)$ the space of square integrable functions, $H^1(\Omega)$ is the space of functions with derivatives in $L^2(\Omega)$. We use the following notation for the L^2 inner product in Q, i.e., $(f,g)_Q = \int_Q f\cdot g\,dQ$. We drop the suffix for $Q \equiv \Omega$, i.e., $(f,g) \equiv (f,g)_Q$. Let $\boldsymbol{\tau}$ and $\boldsymbol{\varepsilon}$ be two second order tensors, we define $\langle\boldsymbol{\tau},\boldsymbol{\varepsilon}\rangle \doteq \int_\Omega \boldsymbol{\tau} : \boldsymbol{\varepsilon}\,d\Omega = \int_\Omega \boldsymbol{\tau}_{ij}\boldsymbol{\varepsilon}_{ij}\,d\Omega$ (Einstein summation applies). Given the vector $\mathbf{v}$, its gradient is denoted as $\nabla\mathbf{v}$ and its ij component is $\frac{\partial\mathbf{v}_i}{\partial x_j}$.

Let $\mathcal{V}$ be an appropriate test space with null traces on Dirichlet boundary conditions, and $\mathcal{U}$ an appropriate trial space. Given the boundary conditions $\overline{\rho}$, $\overline{\mathbf{m}}$, $\overline{T}$, $\overline{\mathbf{B}}$, $\overline{\psi}$ and assuming fluxes are known at Neumann boundaries, the Galerkin weak form reads:

Find $\mathbf{U} \doteq [\rho, \mathbf{m}, T, \mathbf{B}, \psi]^T \in \mathcal{U}$ such that $\rho = \overline{\rho}$ on Γ_D^ρ, $\mathbf{m} = \overline{\mathbf{m}}$ on $\Gamma_D^{\mathbf{m}}$, $T = \overline{T}$ on Γ_D^T, $\mathbf{B} = \overline{\mathbf{B}}$ on $\Gamma_D^{\mathbf{B}}$, $\psi = \overline{\psi}$ on Γ_D^ψ, and

$$\mathcal{A}(\mathbf{W},\mathbf{U}) = \mathcal{F}(\mathbf{W}) \quad \forall\ \mathbf{W} \doteq [q,\mathbf{w},\theta,\mathbf{C},s]^T \in \mathcal{V},$$

where

$$\begin{aligned}\mathcal{A}(\mathbf{W},\mathbf{U}) \doteq\ & (q,\partial_t\rho) - (\nabla q,\mathbf{m}) \\ & + (\mathbf{w},\partial_t\mathbf{m}) - \langle\nabla\mathbf{w},\mathbf{m}\otimes\mathbf{u}\rangle - (\nabla\cdot\mathbf{w},\, p + \tfrac{2}{3Re}(\nabla\cdot\mathbf{u})) + \langle\nabla\mathbf{w},\,\tfrac{1}{Re}(\nabla\mathbf{u}+(\nabla\mathbf{u})^T)\rangle - (\mathbf{w},\mathbf{j}\times\mathbf{B}) \\ & + (\theta,\,\tfrac{n}{\gamma}\partial_t T) + (\theta,\,\tfrac{n}{\gamma}\mathbf{u}\cdot\nabla T) + (\theta,\, nT(\nabla\cdot\mathbf{u})) + (\nabla\theta,\mathbf{q}) - (\theta,\,\tfrac{1}{S}\|\mathbf{j}\|^2) - (\theta,\,\tfrac{1}{Re}\boldsymbol{\pi}:\nabla\mathbf{u}) \\ & + (\mathbf{C},\partial_t\mathbf{B}) - \langle\nabla\mathbf{C},\mathbf{u}\otimes\mathbf{B}-\mathbf{B}\otimes\mathbf{u}\rangle + \left\langle\nabla\mathbf{C},\,\tfrac{1}{S}\left(\nabla\mathbf{B}-(\nabla\mathbf{B})^T\right)\right\rangle - (\nabla\cdot\mathbf{C},\psi) \\ & + (s,\nabla\cdot\mathbf{B}),\end{aligned}$$

and

$$\begin{aligned}\mathcal{F}(\mathbf{W}) \doteq\ & -(q\mathbf{n},\mathbf{m})_{\Gamma_N^\rho} \\ & - \langle\mathbf{n}\otimes\mathbf{w},\mathbf{m}\otimes\mathbf{u}\rangle_{\Gamma_N^{\mathbf{m}}} - (\mathbf{n}\cdot\mathbf{w},\,p)_{\Gamma_N^{\mathbf{m}}} - (\mathbf{n}\cdot\mathbf{w},\,\tfrac{2}{3Re}(\nabla\cdot\mathbf{u}))_{\Gamma_N^{\mathbf{m}}} + \langle\mathbf{n}\otimes\mathbf{w},\,\tfrac{1}{Re}(\nabla\mathbf{u}+(\nabla\mathbf{u})^T)\rangle_{\Gamma_N^{\mathbf{m}}} \\ & + (\mathbf{n}\theta,\mathbf{q})_{\Gamma_N^\theta} \\ & - \langle\mathbf{n}\otimes\mathbf{C},\mathbf{u}\otimes\mathbf{B}-\mathbf{B}\otimes\mathbf{u}\rangle_{\Gamma_N^{\mathbf{B}}} + \left\langle\mathbf{n}\otimes\mathbf{C},\,\tfrac{1}{S}\left(\nabla\mathbf{B}-(\nabla\mathbf{B})^T\right)\right\rangle_{\Gamma_N^{\mathbf{B}}} \\ & - (\mathbf{n}\cdot\mathbf{C},\psi)_{\Gamma_N^\psi}.\end{aligned}$$

It is important to stress that the independent variables are momentum, $\mathbf{m}$, and density ρ. Hence, velocity is a dependent quantity computed as $\mathbf{u} = \mathbf{m}/\rho$. In practice, homogeneous Dirichlet boundary conditions are applied everywhere for ψ, i.e., $\bar{\psi} = 0$ and $\Gamma_D^\psi \equiv \partial\Omega$. That allows to apply perfectly conducting boundary conditions as shown in the following remark.

Remark 2.1. Notice that it can be shown that

$$-\langle\mathbf{n}\otimes\mathbf{C},\mathbf{u}\otimes\mathbf{B}-\mathbf{B}\otimes\mathbf{u}\rangle_{\Gamma_N^{\mathbf{B}}} + \left\langle\mathbf{n}\otimes\mathbf{C},\,\tfrac{1}{S}\left(\nabla\mathbf{B}-(\nabla\mathbf{B})^T\right)\right\rangle_{\Gamma_N^{\mathbf{B}}} = (\mathbf{E}\times\mathbf{n},\mathbf{C})_{\Gamma_N^{\mathbf{B}}}.$$

Therefore, homogeneous Neumann boundary conditions on $\Gamma_N^{\mathbf{B}}$ is equivalent to imposing a perfectly conducting wall.

3. Finite element discretization

The continuous variational problem introduced in Section 2.2 is approximated using the FE method. It is well known that the Galerkin weak form suffers from a number of deficiencies. For incompressible resistive MHD these include the inability to employ equal-order interpolation for velocity/pressure ($\mathbf{u}$, P), and the magnetic inductance/Lagrange multiplier ($\mathbf{B}$, ψ) coupling [4,5,15], as well as the control of unphysical oscillations due to convection and unresolved internal and boundary layers [4,5,14,15]. To develop a stabilized finite-element variational weak form for the variational problem in Section 2.2 that overcomes these deficiencies, a VMS formulation is developed following the general procedures developed and outlined in [5,14,35–37]. In the forthcoming sections, we briefly introduce the stabilization method and the resulting formulation. Before introducing the stabilization method, let us present the discretization used and some useful notation. Let $\mathcal{T}_h$ be a tessellation of Ω in elements K. We use conforming Lagrangian finite element spaces for all unknown, in particular we define $V_h^p \doteq \{v_h \in \mathcal{C}^0 : v_h|_K \in Q_p(K)\ \forall\ K \in \mathcal{T}_h\}$, where Q_p is the space of polynomials of partial degree p.

Moreover, let

$$\begin{aligned}&\mathcal{Q}_h \doteq \{q \in V_h^1(\Omega) : q = 0 \text{ on } \Gamma_D^\rho\},\\ &\mathcal{W}_h \doteq \{\mathbf{w} \in [V_h^1(\Omega)]^d : \mathbf{w} = 0 \text{ on } \Gamma_D^{\mathbf{m}}\},\\ &\vartheta_h \doteq \{\theta \in V_h^2(\Omega) : \theta = 0 \text{ on } \Gamma_D^T\},\\ &\mathcal{C}_h \doteq \{\mathbf{C} \in [V_h^1(\Omega)]^d : \mathbf{C} = 0 \text{ on } \Gamma_D^{\mathbf{B}}\},\\ &\mathcal{S}_h \doteq \{s \in V_h^1(\Omega) : s = 0 \text{ on } \Gamma_D^\psi\},\end{aligned}$$

and, $\mathcal{V}_h \doteq \mathcal{Q}_h \times \mathcal{W}_h \times \vartheta_h \times \mathcal{C}_h \times \mathcal{S}_h$ and $\mathcal{U}_h \doteq V_h^1 \times [V_h^1]^d \times V_h^2 \times [V_h^1]^d \times V_h^1$.

Remark 3.1. In this study, a linear discretization for all unknowns is used, except for temperature, T. Instead, temperature is discretized with a quadratic interpolation, to improve the accuracy of highly anisotropic thermal conductivities. Other authors suggest mixed formulations or even higher polynomial orders to accurately transport the energy (see [30,38–40] and references therein). Our current formulation does allow for higher-order interpolation of nodal FE unknowns ($\leq$ 9th order) and planned follow on studies will consider the issue of anisotropic heat transport in more detail.

3.1. Variational multiscale discretization

The VMS formulation is based in the additive splitting of the solution in two distinct spaces: the resolved representation of $\mathbf{U}$, in this case the FE solution, $\mathbf{U}_h$, and its unresolved portion $\mathbf{U}'$ [35–37]. Therefore, the space is decomposed as $\mathcal{U} = \mathcal{U}_h + \mathcal{U}'$ and similarly for $\mathbf{W} = \mathbf{W}_h + \mathbf{W}'$ and $\mathcal{V} = \mathcal{V}_h + \mathcal{V}'$. Hence, since $\mathcal{A}(\mathbf{W}, \mathbf{U})$ is linear with respect to $\mathbf{W}$ we have the following weak forms

$$\mathcal{A}(\mathbf{W}_h, \mathbf{U}_h + \mathbf{U}') = \mathcal{F}(\mathbf{W}_h) \quad \forall\ \mathbf{W}_h \in \mathcal{V}_h \tag{4a}$$

$$\mathcal{A}(\mathbf{W}', \mathbf{U}_h + \mathbf{U}') = \mathcal{F}(\mathbf{W}') \quad \forall\ \mathbf{W}' \in \mathcal{V}' \tag{4b}$$

The unresolved scales $\mathbf{U}'$ are not found using Eq. (4b), instead approximated using a given closure. Different VMS formulations can be devised depending on the closure definition [41]. In the present work, the formulation developed for incompressible MHD in [5] is extended to low Mach number thermally coupled compressible MHD. Following that work, $\mathbf{U}'$ is approximated as $\mathbf{U}' \approx -\boldsymbol{\tau}\mathbf{P}\mathcal{R}(\mathbf{U}_h)$, where $\boldsymbol{\tau}$ is a diagonal matrix of stabilization parameters, $\mathbf{P}$ is a projector operator onto the sub-grid scale, and $\mathcal{R}(\mathbf{U}_h)$ is the strong residual, i.e., Eqs. (3).

Remark 3.2. Strong consistency is ensured by definition, since $\mathbf{U}'$ approximation is based in the strong form residual of (3). Hence, if $\mathbf{U}_h$ is equal to the exact solution $\mathbf{U}' = 0$, and thus, all stabilization terms become null.

In order to obtain a closed form for the terms $\mathcal{A}(\mathbf{W}_h, \mathbf{U}')$ a series of assumptions are taken based on [5,35,37,42,43]. The unresolved scales are considered local and non-zero only in the interior of the elements, i.e, $\mathbf{U}' = 0$ on ∂K. Higher order terms are neglected, e.g., $u' \cdot \rho' \approx 0$. Nearly incompressible flows are assumed, i.e., $\nabla \cdot \mathbf{u} \approx 0$. The time variation of unresolved scales is neglected, i.e., $\partial_t \mathbf{U}' = 0$. The identity matrix is used as the projector operator, $\mathbf{P} = \mathbf{I}$. Following the standard steps to obtain a VMS formulation and keeping all terms would lead to a fully coupled stabilization term. However, the formulation developed in this work only preserves the convective stabilization terms, the saddle point ones, and a novel stabilization term for nearly incompressible flows.

The component-wise fluctuations are approximated in terms of the residuals interior to the elements,

$$\rho' \approx -\tau_{\mathbf{m}} R_h^c, \quad \mathbf{u}' \approx -\tau_{\mathbf{m}} \tfrac{R_h^{\mathbf{m}}}{\rho}, \quad p' \approx -\tau_p R_h^p, \quad T' \approx -\tau_T R_h^T, \quad \mathbf{B}' \approx -\tau_B R_h^{\mathbf{B}}, \quad \psi' \approx -\tau_\psi R_h^\psi,$$

where the stabilization parameters $\tau_{\mathbf{m}}$, τ_p, τ_T, τ_B, and τ_ψ are defined as algebraic approximations of the inverse of the differential operator, which (in dimensionless form) read

$$\tau_{\mathbf{m}} \doteq \left[C_1^{\mathbf{m}} \left(\frac{2}{\Delta t} \right)^2 + C_2^{\mathbf{m}} \mathbf{u} \cdot \mathbf{G}\mathbf{u} + C_3^{\mathbf{m}} \mathbf{B} \cdot \mathbf{G}\mathbf{B} + C_4^{\mathbf{m}} \frac{\mu^2}{n^2} \|\mathbf{G}\|^2 \right]^{-1/2},$$

$$\tau_p \doteq (tr(\mathbf{G})\tau_{\mathbf{m}})^{-1},$$

$$\tau_T \doteq \left[C_1^T \left(\frac{\rho}{\Delta t} \right)^2 + C_2^T n^2 \mathbf{u} \cdot \mathbf{G}\mathbf{u} + C_3^T \mathbf{B} \cdot \mathbf{G}\mathbf{B} + C_4^T \kappa^2 \|\mathbf{G}\|^2 \right]^{-1/2},$$

$$\tau_{\mathbf{B}} \doteq \left[C_1^{\mathbf{B}} \left(\frac{2}{\Delta t} \right)^2 + C_2^{\mathbf{B}} \mathbf{u} \cdot \mathbf{G}\mathbf{u} + C_3^{\mathbf{B}} \mathbf{B} \cdot \mathbf{G}\mathbf{B} + C_4^{\mathbf{B}} \frac{\eta^2}{\mu_0^2} \|\mathbf{G}\|^2 \right]^{-1/2},$$

$$\tau_\psi \doteq (tr(\mathbf{G})\tau_{\mathbf{B}})^{-1}.$$

where C_i^α are constants independent of the mesh, and $\mathbf{G}$ is the contravariant metric tensor of the transformation from local element coordinates, ζ_α to physical coordinates, x_i, $\mathbf{G}_{ij} = \frac{\partial \zeta_\alpha}{\partial x_i} \frac{\partial \zeta_\alpha}{\partial x_j}$. The strong form residuals correspond to Eqs. (3a) to (3e), respectively, and $R_h^P = R_h^c$. Notice that the term $C_3^T \mathbf{B} \cdot \mathbf{G}\mathbf{B}$ is not motivated from the attempt of approximating the inverse of the differential operator. Instead, it is included to use a similar approximation of the convective term as for $\tau_{\mathbf{B}}$ and $\tau_{\mathbf{m}}$, which numerical experiments suggest an improvement of the stability.

Remark 3.3. The following modifications are introduced for the nearly incompressible regime

- *Density*: the standard VMS term for continuity is $(\nabla q_h, \mathbf{m}')$. Instead, following [23,24] and treating $\mathbf{m}$ as $\rho \cdot \mathbf{u}$ separately, yields $(\nabla q_h, \rho_h \mathbf{u}') + (\nabla q_h, \mathbf{u}_h \rho')$. The first term is equivalent to the standard term and contains saddle point stabilizing term $(\nabla q_h, \nabla p)$, which gives control on the pressure, additionally the second contains the term $(\mathbf{u}_h \cdot \nabla q_h, \mathbf{u}_h \cdot \nabla \rho_h)$ which improves the convective stabilization regardless of the value of $\nabla \cdot \mathbf{u}$.
- *Momentum*: for the momentum equation it is important to approximate $p' \approx \tau_p R_h^c$, which results in a term of the form $(\nabla \cdot \mathbf{w}_h, \nabla \cdot \mathbf{m}_h)$, providing control over the momentum divergence and improves the stabilization for highly convected flows [44].

Therefore, the resulting terms after approximating the subscale unknowns by the residual-based approximation reads

$$(\nabla q_h, \tau_m R^m) + (\mathbf{u}_h \cdot \nabla q_h, \tau_m R^c) + (\mathbf{u}_h \cdot \nabla \mathbf{w}_h, \tau_m R^m) + (\mathbf{u}_h \cdot \nabla \mathbf{w}_h, \tau_m R^c) + (\nabla \cdot \mathbf{w}_h, \tau_p R^c),$$

where the first and last term provide control of the saddle point problem, and the second and third are the convective stabilization terms.

After adding the stabilization terms the variational form reads

$$\begin{aligned} \mathcal{A}(\mathbf{W}_h, \mathbf{U}_h + \mathbf{U}') = \mathcal{A}(\mathbf{W}_h, \mathbf{U}_h) - \sum_{K \in \mathcal{T}_h} \big(& (\nabla q_h, \rho_h \mathbf{u}' + \mathbf{u}_h \rho')_K \\ & + \langle \nabla \mathbf{w}_h, \rho \mathbf{u}' \otimes \mathbf{u}_h + \rho' \mathbf{u}_h \otimes \mathbf{u}_h \rangle_K + (\nabla \cdot \mathbf{w}_h, p')_K \\ & + (\nabla \theta_h, \overline{\gamma}^{-1} \mathbf{u}_h T')_K \\ & + \langle \nabla \mathbf{C}_h, \mathbf{u}_h \otimes \mathbf{B}' - \mathbf{B}' \otimes \mathbf{u}_h \rangle_K + (\nabla \cdot \mathbf{C}_h, \psi')_K \\ & + (\nabla s_h, \mathbf{B}')_K \big) \end{aligned} \tag{5}$$

Note that for practical reasons only the ideal terms of (3) have been included. This is common practice and consistent when linear FE are used, since second derivatives are null in the interior of the elements [5]. For higher order FE non-ideal terms do not vanish, however in highly convective flows non-ideal terms contribution to the residual is small compared with the ideal terms. This contribution has been neglected for the temperature equation.

Remark 3.4. Here the reduced VMS weak form includes contributions from:

- the Galerkin form in Section 2.2 (first line, right hand side),
- a Streamline Upwind Petrov–Galerkin (SUPG) tensor operator to stabilize convective effects for momentum (second line, first term),
- a cross coupling $(\mathbf{u}, P)$ commonly included at higher Reynolds numbers for Navier–Stokes (second line, second term),
- the pressure–velocity stabilization term that eliminates oscillatory modes from the null space of the incompressible Navier–Stokes operators for the $(\mathbf{u}, P)$ coupling to allow stable equal-order interpolation (second line, third term),
- the SUPG type operator for convection effects in the temperature equation (third line)
- the SUPG tensor type operators for the divergence form of convection in the induction equation (fourth line, first term),
- the weak divergence type Laplacian operator cross-coupling term for $(\mathbf{B}, \psi)$ that further enhances the invertibility of the induction equation (fourth line, second term),
- and the induction-Lagrange multiplier stabilization term that eliminates oscillatory modes from the null space of the induction/solenoidal constraint equations for the $(\mathbf{B}, \psi)$ coupling to allow stable equal-order interpolation (fifth line).

3.2. Discontinuity capturing operator

The convection stabilizing terms included in (5) can be seen as residual-based streamline diffusion operators. For problems with very strong unresolved gradients or possible shocks in the solution it is necessary to include

crosswind diffusion. Therefore, we supplement our formulation with discontinuity capturing type operators. The terms included are based on Guermond et al. [45]. They propose an operator that is driven by the entropy and PDE residuals. These quantities are expected to be larger in regions where there exist large gradients. Hence, the idea is to concentrate the action of the operator in these areas.

Let $K \in \mathcal{T}_h$ be an arbitrary element of the mesh, we denote by $\mathcal{G}^K$ the set of integration points for element K. In addition, we define $\mathcal{N}$ to be set of nodes in $\mathcal{T}_h$. For any variable, $v_h \in V_h^p$, we denote its value at a given coordinate, $\boldsymbol{x}_i$, as $v_i \doteq v_h(\boldsymbol{x}_i)$, where i can be a node ($i \in \mathcal{N}$) or an integration point ($i \in \mathcal{G}^K$). The modified form reads

$$\tilde{\mathcal{A}}(\mathbf{W}_h, \mathbf{U}_h + \mathbf{U}') \doteq \mathcal{A}(\mathbf{W}_h, \mathbf{U}_h + \mathbf{U}') + \mathcal{B}(\mathbf{W}_h, \mathbf{U}_h)$$

where

$$\mathcal{B}(\mathbf{W}_h, \mathbf{U}_h) \doteq \sum_{K \in \mathcal{T}_h} (\nabla q_h, \nu_{LLF}^K \nabla \rho_h)_K + (\nabla \mathbf{w}_h, \tfrac{1}{2}\nu_{\mathbf{m}}^K (\nabla \mathbf{u}_h + (\nabla \mathbf{u}_h)^T))_K + (\tfrac{\mathbf{B}}{\|\mathbf{B}\|} \cdot \nabla \theta_h, \tfrac{u_A h}{2} \tfrac{\mathbf{B}}{\|\mathbf{B}\|} \cdot \nabla T_h)_K.$$

The artificial viscosity value ν_m^K is defined as

$$\nu_m^K = \rho_{\max} \min(\nu_{LLF}^K, \nu_S^K),$$

where

$$\nu_{LLF}^K = \max_{i \in \mathcal{G}^K} \left(C_{LLF} h \left(\sqrt{c_i^2 + u_{A_i}^2} + \|\mathbf{u}_i\| \right) \right)$$

where h is the local mesh size, c_i is the sound speed at integration point $\boldsymbol{x}_i$, $c_i = \sqrt{\frac{\gamma p_i}{\rho_i}}$, and u_{A_i} is the Alfvèn speed at the integration point $\boldsymbol{x}_i$, $u_{A_i} = \frac{\|B_i\|}{\sqrt{\rho_i}}$. Notice all quantities in this section are computed using dimensionless values, hence it is expected that $u_{A_i} \sim 1$. $C_{LLF} = 1/2$, and $C_{\max} = 2$ are user-defined constants to modulate the action of the discontinuity capturing operator. The entropy viscosity is defined as

$$\nu_S^K = \max_{i \in \mathcal{G}^K} \left(C_{\max} h^2 \max \left(\frac{\|R_i^S\|}{\hat{S}}, \frac{S_i}{\rho_i} \frac{\|R_i^c\|}{\hat{S}} \right) \right)$$

where R_i^c is the continuity residual, R_i^S is the entropy residual, and S_i is the entropy $S_i = \rho \ln \left(\rho_0^{\overline{\gamma}} u_0^2 \frac{p_i}{\rho_i^{\overline{\gamma}}} \right)$. Using the definition of the entropy residual for resistive MHD [46]

$$R_i^S = \frac{\partial S_i}{\partial t} + S_i(\nabla \cdot \mathbf{u}_i) + \mathbf{u}_i \cdot \nabla S_i + \mu_0 \overline{\gamma} \frac{\rho_i}{p_i} (\mathbf{u}_i \cdot \mathbf{B}_i)(\nabla \cdot \mathbf{B}_i)$$

where the time derivative of entropy is obtained by

$$\frac{\partial S_i}{\partial t} = \left[\left(\ln \left(\rho_0^{\overline{\gamma}} u_0^2 \tfrac{p_i}{\rho_i} \right) - \gamma \right) \frac{\partial \rho_i}{\partial t} + \frac{\rho_i}{p_i} \frac{\partial p_i}{\partial t} \right].$$

The global entropy scaling, $\hat{S}$, is computed as follows

$$\hat{S} = \max \left(|S_{\max} - \overline{S}|, |S_{\min} - \overline{S}| \right), \text{ with } \overline{S} = \frac{\int_\Omega S d\Omega}{\int_\Omega d\Omega}, \quad S_{\max} = \max_{i \in \mathcal{N}} S_i, \quad S_{\min} = \min_{i \in \mathcal{N}} S_i.$$

Finally, the stabilized problem reads: Find $\mathbf{U}_h \doteq [\rho_h, \mathbf{m}_h, T_h, \mathbf{B}_h, \psi_h]^T \in \mathcal{U}_h$ such that $\rho_h = \overline{\rho}$ on Γ_D^ρ, $\mathbf{m}_h = \overline{\mathbf{m}}$ on $\Gamma_D^{\mathbf{m}}$, $T_h = \overline{T}$ on Γ_D^T, $\mathbf{B}_h = \overline{\mathbf{B}}$ on $\Gamma_D^{\mathbf{B}}$, $\psi_h = \overline{\psi}$ on Γ_D^ψ, and

$$\tilde{\mathcal{A}}(\mathbf{W}_h, \mathbf{U}_h + \mathbf{U}') = \mathcal{F}(\mathbf{W}_h) \quad \forall\ \mathbf{W}_h \doteq [q_h, \mathbf{w}_h, \theta_h, \mathbf{C}_h, s_h]^T \in \mathcal{V}_h.$$

Remark 3.5. For the sake of simplicity, only the "plasma" domain Ω has been considered for the discussion of the formulation. However, it is possible to extend the above formulation to multiple domains. In Section 5.2, an example where the walls are included in the simulation domain is given. Let Ω' be domain containing Ω and extending over the walls, such that $\Omega \subset \Omega'$. Let $\Omega^w = \Omega' \backslash \Omega$ be the wall subdomain. Then, the above discrete spaces for density,

momentum, temperature, magnetic field, and Lagrange multiplier spaces are redefined as

$$\mathcal{Q}'_h \doteq \{q \in V_h^1(\Omega') : q = 0 \text{ on } \Gamma_D^{\rho} \cup \Omega^w\},$$
$$\mathcal{W}'_h \doteq \{\mathbf{w} \in [V_h^1(\Omega')]^d : \mathbf{w} = 0 \text{ on } \Gamma_D^{\mathbf{m}} \cup \Omega^w\},$$
$$\vartheta'_h \doteq \{\theta \in V_h^2(\Omega') : \theta = 0 \text{ on } \Gamma_D'^{T}\},$$
$$\mathcal{C}'_h \doteq \{\mathbf{C} \in [V_h^1(\Omega')]^d : \mathbf{C} = 0 \text{ on } \Gamma_D'^{\mathbf{B}}\},$$
$$\mathcal{S}'_h \doteq \{s \in V_h^1(\Omega') : s = 0 \text{ on } \Gamma_D'^{\psi}\},$$

where, as before, $\Gamma_D'^{\alpha}$ represents the portion of $\partial\Omega'$ where Dirichlet boundary conditions are imposed for the unknown α, and similarly, $\Gamma_N^{\alpha} = \partial\Omega' \backslash \Gamma_D'^{\alpha}$ denotes the portion of $\partial\Omega'$ where Neumann boundary conditions are imposed. Let $\overline{V}_h^1 \doteq \{v \in V_h^1 : v = 0 \in \Omega^w\}$. Finally, the test and trial spaces can be redefined as $\mathcal{V}_h \doteq \mathcal{Q}'_h \times \mathcal{W}'_h \times \vartheta'_h \times \mathcal{C}'_h \times \mathcal{S}'_h$, and $\mathcal{U} \doteq \overline{V}_h^1(\Omega') \times [\overline{V}_h^1(\Omega')]^d \times V_h^2(\Omega') \times [V_h^1(\Omega')]^d \times V_h^1(\Omega')$. Notice, that in Ω^w the Eqs. (3a)–(3b) are not solved since the test functions are null, and the convective terms in (3c)–(3e) vanish.

3.3. Discrete from of the linearized system

The stabilized weak form is linearized using Newton's method, the discrete linear system can be expressed as the following 5×5 block linear system,

$$\begin{bmatrix} \mathrm{F}_{\mathbf{m}} & \tilde{\mathrm{B}}^{\mathrm{T}}_{\mathbf{m},\boldsymbol{\rho}} & \mathbf{C}_{\mathbf{m},\mathbf{T}} & \mathbf{Z} & \mathbf{0} \\ \mathrm{B}_{\boldsymbol{\rho},\mathbf{m}} & \mathrm{F}_{\rho} & \mathbf{C}_{\rho,\mathbf{T}} & \mathbf{0} & \mathbf{0} \\ \mathbf{A}_{\mathbf{T},\mathbf{m}} & \mathbf{C}_{\mathbf{T},\rho} & \mathrm{F}_{\mathrm{T}} & \mathbf{Z}_{\mathbf{T}} & \mathbf{0} \\ \mathbf{Y} & \mathbf{C}_{\mathbf{B},\rho} & \mathbf{0} & \mathbf{F}_{\mathbf{B}} & \mathbf{B}_{\mathbf{B}}{}^{T} \\ \mathbf{C}_{\boldsymbol{\psi},\mathbf{m}} & \mathbf{C}_{\boldsymbol{\psi},\rho} & \mathbf{0} & \mathbf{B}_{\mathbf{B}} & \mathbf{L}_{\boldsymbol{\psi}} \end{bmatrix} \begin{bmatrix} \boldsymbol{\delta}\hat{\mathbf{m}} \\ \delta\hat{\rho} \\ \delta T \\ \boldsymbol{\delta}\hat{B} \\ \delta\hat{\boldsymbol{\psi}} \end{bmatrix} = - \begin{bmatrix} \mathbf{r}_{\mathbf{m}} \\ \mathrm{r}_{\rho} \\ \mathrm{r}_{T} \\ \mathbf{r}_{B} \\ \mathrm{r}_{\boldsymbol{\psi}} \end{bmatrix},$$

where the matrix $\mathrm{F}_{\mathbf{m}}$ corresponds to the discrete transient, convection, diffusion and stress terms acting on the momentum unknowns $\boldsymbol{\delta}\hat{\mathbf{m}}$, similarly the matrix F_{ρ} corresponds to the density unknowns, $\delta\hat{\rho}$, similarly the matrix F_{T} corresponds to the temperature unknowns, δT, the matrix $\mathbf{F}_{\mathbf{B}}$ corresponds to the magnetics unknowns $\boldsymbol{\delta}\hat{\mathbf{B}}$, and finally the matrix $\mathbf{L}_{\boldsymbol{\psi}}$ corresponds to the stabilization Laplacian and acts on the Lagrange multipliers $\boldsymbol{\delta}\hat{\boldsymbol{\psi}}$. The δ terms contain Newton updates to the corresponding variables.

In order to facilitate the block preconditioner discussion below, here the momentum and density is treated as strongly coupled in a 2×2 system, these are considered as a single operator. Thus, the single Navier–Stokes-like flow operator, reads

$$\mathbf{F}_{\mathrm{ns}} := \begin{bmatrix} \mathrm{F}_{\mathbf{m}} & \tilde{\mathrm{B}}^{\mathrm{T}}_{\mathbf{m},\boldsymbol{\rho}} \\ \mathrm{B}_{\boldsymbol{\rho},\mathbf{m}} & \mathrm{F}_{\rho} \end{bmatrix},$$

with the corresponding off-diagonal blocks:

$$\mathbf{Z}_{\mathrm{ns}} = \begin{bmatrix} \mathbf{Z} \\ \mathbf{0} \end{bmatrix}, \quad \mathbf{Y}_{\mathrm{ns}} = \begin{bmatrix} \mathbf{Y} & \mathbf{C}_{\mathbf{B},\rho} \end{bmatrix}, \quad \mathbf{C}_{\mathrm{ns}} = \begin{bmatrix} \mathbf{C}_{\boldsymbol{\psi},\mathbf{m}} & \mathbf{C}_{\boldsymbol{\psi},\rho} \end{bmatrix}, \quad C_T = \begin{bmatrix} \mathbf{C}_{\mathbf{m},\mathbf{T}} \\ \mathbf{C}_{\rho,\mathbf{T}} \end{bmatrix}, \quad A_T = \begin{bmatrix} \mathbf{A}_{\mathbf{T},\mathbf{m}} & \mathbf{C}_{\mathbf{T},\rho} \end{bmatrix}.$$

With this change of notation, and a slight reordering of variables, the linearized Jacobian 4×4 block system reads

$$\begin{bmatrix} \mathbf{F}_{\mathbf{B}} & \mathbf{B}_{\mathbf{B}}{}^{T} & \mathbf{Y}_{\mathrm{ns}} & \\ \mathbf{B}_{\mathbf{B}} & \mathbf{L}_{\boldsymbol{\psi}} & \mathbf{C}_{\mathrm{ns}} & \\ \mathbf{Z}_{\mathrm{ns}} & & \mathbf{F}_{\mathrm{ns}} & C_T \\ \mathbf{Z}_T & & A_T & \mathrm{F}_{\mathrm{T}} \end{bmatrix}.$$

4. Fully-implicit time integration and strongly-coupled multiphysics block preconditioned Newton-Krylov solver

4.1. Fully-implicit time integration and strongly-coupled Newton-Krylov solver

The low-Mach number compressible MHD equations in (3a), supports a number of fast time-scales. These include elliptic effects due to the solenoidal involution of the magnetic field and the nearly incompressible flow

response at low Mach numbers, fast time-scale parabolic effects due to momentum and magnetic diffusion, and fast Alfvén wave propagation. This system can exhibit behavior that is characterized by widely separated time-scales as well as overlapping time-scales. These characteristics make the robust and efficient iterative solution of these systems very challenging. In this context fully-implicit methods are an attractive choice that can often provide robust time integration techniques. These methods can be designed with various types of stability properties that allow robust integration of multiple-time-scale systems without the requirement to resolve the stiff modes of the system (which are not of interest since they do not control the accuracy of time integration). In the computations presented in this study, a fully-implicit multistage singly diagonal implicit Runge–Kutta (SDIRK) method is employed to accurately and efficiently integrate the time evolution of the MHD system. Specifically the 2-stage, second order SDIRK22. More details on the fully-implicit integration and example order-of-accuracy verification results can be found in [4,5])

The governing equations discretized by the finite element method result in a very large-scale, coupled highly nonlinear algebraic system(s) that must be solved. Solution of these systems places a heavy burden on both the nonlinear and linear solvers and require robust, scalable, and efficient methods. In this study Newton-based iterative nonlinear solvers [47] are employed. These solvers can exhibit quadratic convergence rates independent of problem size when sufficiently robust linear solvers are available. For the latter, we employ Krylov iterative techniques. A Newton–Krylov (NK) method is an implementation of Newton's method in which a Krylov iterative solution technique is used to approximately solve the linear systems, $\mathbf{J}_k\mathbf{s}_{k+1} = -\mathbf{F}_k$, that are generated at each step of Newton's method. For efficiency, an inexact Newton method [47,48] is usually employed, whereby one approximately solves the linear systems generated in the Newton method by choosing a forcing term η_k and stopping the Krylov iteration when the inexact Newton condition, $\|\mathbf{F}_k+\mathbf{J}_k\mathbf{s}_{k+1}\| \leq \eta_{k+1}\|\mathbf{F}_k\|$ is satisfied. The particular Krylov method that is used in this study is a robust non-restarted GMRES method that is capable of iteratively converging to the solution of very large non-symmetric linear systems such as developed from the discretized equations, provided a sufficiently robust and scalable preconditioning method is available [4,5,49–52].

4.2. Overview of multiphysics approximate block preconditioners

In order to solve the linear systems $\mathbf{J}_k\mathbf{s}_{k+1} = -\mathbf{F}_k$ efficiently, we use a physics-based preconditioning strategy based on segregating the degrees of freedom [53]. The solution vector can be decomposed into its individual degree of freedom components as $\mathbf{s} = (\mathbf{B}, \psi, \mathbf{s}_{\rm ns}, T)$, where $\mathbf{s}_{\rm ns} = (\rho\mathbf{u}, \rho)$ represents the fluid degrees of freedom. In the blocking of the multiphysics system there are two important aspects for the choice of how the block decomposition proceeds. The first is that in the plasma region all the balance equations are active (and therefore all the unknowns), and in the solid and vacuum regions only the magnetic induction, Lagrange multiplier, and temperature equations/unknowns are solved. Further, $\rho\mathbf{u}$, ρ, $\mathbf{B}$ and ψ are all interpolated with a linear approximation, whereas T is discretized with quadratic elements, so it is important to block these degrees of freedom apart to use solvers tailored to each discretization. Using this degree of freedom blocking, the Jacobian update equation can be represented in the form

$$\begin{bmatrix} \mathbf{F_B} & \mathbf{B_B}^T & \mathbf{Y}_{\rm ns} & \\ \mathbf{B_B} & \mathbf{L}_{\boldsymbol{\psi}} & \mathbf{C}_{\rm ns} & \\ \mathbf{Z}_{\rm ns} & & \mathbf{F}_{\rm ns} & C_T \\ \mathbf{Z}_T & & A_T & \mathrm{F_T} \end{bmatrix} \begin{bmatrix} \mathbf{B} \\ \psi \\ \mathbf{s}_{\rm ns} \\ T \end{bmatrix} = - \begin{bmatrix} \mathbf{f_B} \\ \mathbf{f}_{\psi} \\ \mathbf{f}_{\rm ns} \\ \mathbf{f}_T \end{bmatrix}.$$

In this form, each block represents a different physical operator, and we can exploit the physics-based structure to develop effective approximations. The operators on the block diagonal $\mathbf{F_B}$, $\mathbf{L}_{\boldsymbol{\psi}}$, $\mathbf{F}_{\rm ns}$ and $\mathrm{F_T}$ correspond to the transient magnetic convection–diffusion type operators, a Laplacian operator on the Lagrange multiplier space resulting from stabilization, the $\rho\mathbf{u} - \rho$ Navier–Stokes system, and a transient convection–diffusion operator for the temperature, respectively. Efficient multilevel methods already exist for each of these operators [54]. Off-diagonal terms represent coupling between degrees of freedom. Notably, $\mathbf{Z}_{\rm ns}$ represents the Lorentz force, and $\mathbf{Y}_{\rm ns}$ represents the coupling of $\rho\mathbf{u}$ in the induction equation. The coupling of these operators results into Alfvén wave time-scales. $\mathbf{B_B}$ is the divergence and $\mathbf{B_B}^T$ is the gradient. The elliptic coupling of these operators between $\mathbf{B}$ and ψ results in an infinite time-scale that requires implicit representation.

The particular block preconditioner employed here is a combination of splitting the temperature block away from the other degrees of freedom using the block Jacobi method and a variation of the 3×3 approximate

block factorization (ABF) developed for resistive MHD systems in [50]. At the time-scales of interest, the coupling between temperature and momentum is a one-way non-stiff coupling. Numerical experiments have shown that this approach is as effective as more costly alternatives of treating this splitting with an approximate Schur complement type method. The 3×3 ($\mathbf{B}$, ψ, $\mathbf{s}_{ns}$) system admits the ABF

$$\mathcal{M}_{ABF} = \begin{bmatrix} \mathbf{F_B} & & \mathbf{Y}_{\rm nst} \\ & \mathbf{I} & \\ \mathbf{Z}_{\rm ns} & & \mathbf{F}_{\rm nst} \end{bmatrix} \begin{bmatrix} \mathbf{F_B}^{-1} & & \\ & \mathbf{I} & \mathbf{C}_{\rm nst} \\ & & \mathbf{I} \end{bmatrix} \begin{bmatrix} \mathbf{F_B} & \mathbf{B_B}^T & \\ \mathbf{B_B} & \mathbf{L}_{\psi} & \\ & & \mathbf{I} \end{bmatrix} = \begin{bmatrix} \mathbf{F_B} & \mathbf{B_B}^T & \mathbf{Y}_{\rm nst} \\ \mathbf{B_B} & \mathbf{L}_{\psi} & \mathbf{C}_{\rm nst} \\ \mathbf{Z}_{\rm ns} & \mathbf{Z}_{\rm ns}\mathbf{F_B}^{-1}\mathbf{B_B}^T & \mathbf{F}_{\rm nst} \end{bmatrix}.$$

The strength of this ABF is that it decomposes the 3×3 system into two 2×2 systems which are easier to handle. From a physics-based perspective, the first 2×2 system captures the Alfvén coupling between $\rho\mathbf{u}$ and $\mathbf{B}$, and the second 2×2 system represents the elliptic coupling of $\mathbf{B}$ and ψ. In this way, the ABF corresponds to an operator split approach to decoupling the full system. Any error in the factorization itself is due to the structural perturbation $\mathbf{Z}_{\rm ns}\mathbf{F_B}^{-1}\mathbf{B_B}^T$. It can be shown that in physical regimes of interest that the magnitude of this operator is small and controlled under mesh refinement and increasing time step [53].

In practice, LU factorizations are applied to the 2×2 systems to break them each into two solves on the block diagonal. Then the inverse action of the preconditioner can be represented as

$$\mathcal{M}^{-1} = \begin{bmatrix} \mathbf{F_B} & \mathbf{B_B}^T & \\ & S_L & \\ & & \mathbf{I} \\ & & & \mathbf{I} \end{bmatrix}^{-1} \begin{bmatrix} \mathbf{I} & & & \\ -\mathbf{B_B}\mathbf{F_B}^{-1} & \mathbf{I} & & \\ & & \mathbf{I} & \\ & & & \mathbf{I} \end{bmatrix} \begin{bmatrix} \mathbf{I} & & \mathbf{Y}_{\rm ns} & \\ & \mathbf{I} & \mathbf{C}_{\rm ns} & \\ & & S_{ns} & \\ & & & \mathbf{I} \end{bmatrix}^{-1} \begin{bmatrix} \mathbf{I} & & & \\ & \mathbf{I} & & \\ & & \mathbf{I} & \\ & & & \mathrm{F_T}^{-1} \end{bmatrix}$$

where the Schur complements are defined as

$$S_{ns} = \mathbf{F}_{\rm ns} - \mathbf{Z}_{\rm ns}\mathbf{F_B}^{-1}\mathbf{Y}_{\rm ns}, \qquad S_L = \mathbf{L}_{\psi} - \mathbf{B_B}\mathbf{F_B}^{-1}\mathbf{B_B}^T.$$

Note that one of the lower triangular inverses was omitted without affecting the spectrum of the preconditioned operator [55]. For forming the Schur complements, we approximate the embedded inverses with the absolute row sum inverse (i.e. a SIMPLEC approximation [56]) such that

$$S_{ns} = \mathbf{F}_{\rm ns} - \mathbf{Z}_{\rm ns}(\mathrm{absrowsum}(\mathbf{F_B}))^{-1}\mathbf{Y}_{\rm ns}, \qquad S_L = \mathbf{L}_{\psi} - \mathbf{B_B}(\mathrm{absrowsum}(\mathbf{F_B}))^{-1}\mathbf{B_B}^T.$$

In practice, these approximate Schur complements capture their respective physics well and result in good preconditioner performance. Each inverse operation $\mathbf{F_B}^{-1}$, S_L^{-1}, S_{ns}^{-1}, $\mathrm{F_T}^{-1}$ is the application of one V-cycle of an algebraic multigrid method with an incomplete factorization smoother [53,57].

4.3. Nonlinear and linear convergence criteria

To complete the description of the numerical method that is employed in this study the convergence criteria that are used to determine convergence of the nonlinear/linear iterative methods must be stated. Two nonlinear solver convergence criteria are employed. The first is a requirement of sufficient reduction in the relative nonlinear residual norm, e.g., $\|F_k\|/\|F_o\| < 10^{-2}$, where $\|F_o\|$ is the residual of the initial nonlinear guess. In general, this requirement is set to be easily satisfied. Numerical experiments usually achieve $\|F_k\|/\|F_o\| \lesssim 10^{-6}$, once the second criterion is fulfilled. The second convergence criterion is based on a sufficient decrease of a weighted norm of the relative size of the Newton update vector. The latter criterion requires that the correction, $\Delta\chi_i^k$, for any grid point unknown, χ_i, is small compared to its magnitude, $\left|\chi_i^k\right|$, and is given by

$$\sqrt{\frac{1}{N_u}\sum_{i=1}^{N_u}\left[\frac{|\Delta\chi_i|}{\varepsilon_r\,|\chi_i| + \varepsilon_a}\right]^2} < 1.$$

Here N_u is the total number of unknowns, ε_r is the relative error tolerance between the variable correction and its magnitude, and ε_a is the absolute error tolerance of the variable correction, which sets the magnitude of components that are to be considered to be numerically zero. In this study, the relative-error and absolute-error tolerance are 10^{-3} and 10^{-6} respectively. In practice this criteria controls convergence of the nonlinear solver to sufficient accuracy. Finally in each Newton sub-step the linear system is solved to a relative tolerance of $\eta = 10^{-4}$ with the knowledge that the overall accuracy of the solution for each time step is controlled as described above for convergence of the Newton step [5,49].

5. Numerical results

In this section different numerical tests are performed, which demonstrate the properties of the developed formulation. A 2D Cartesian tearing mode instability is firstly used to verify the scheme and the effectiveness of the stabilization correction. A full 3D simulation of a VDE is performed to assess the effectiveness of the scheme for longer timescale simulations, and a brief scalability overview. Finally, a (1,1)-mode kink instability is performed showing that the formulation is able to handle a 3D instability with complex magnetic field topologies.

5.1. 2D tearing mode

The first numerical test consists on the simulation of resistive instability, i.e., a tearing mode, solved in two dimensions. This problem is initialized with a Harris current sheet and a perturbation that triggers the tearing of the thin current sheet and the growth of a magnetic island. The initial width, δ, of the current sheet and the Lundquist number, S, determine the growth rate of the instability [1]. In [1] it is modeled using an incompressible reduced MHD formulation, since $\nabla\cdot\mathbf{u} \approx 0$. Hence, it becomes a good example for testing the low Mach number stabilization introduced in Section 2.

The problem is solved in $\Omega = [0, 4] \times [-0.5, 0.5]$, discretized in a Cartesian grid with 100×50 elements. The Reynolds number is fixed for all tests to 10^3, and an isotropic thermal conductivity $\kappa = 1$ is considered. The initial conditions for the test read

$$
\begin{aligned}
\rho &= \rho_0 + \frac{1}{2\cosh^2(y/\delta)},\\
\mathbf{m} &= \mathbf{0},\\
T &= 1,\\
B_x &= \frac{\sinh(y/\delta)}{\cosh(y/\delta)} + \frac{\delta_B \pi}{L_y}\cos\left(2\pi\tfrac{x}{L_x}\right)\sin\left(\pi\tfrac{y}{L_y}\right),\\
B_y &= \frac{-2\cdot\delta_B\pi}{L_x}\sin\left(2\pi\tfrac{x}{L_x}\right)\cos\left(\pi\tfrac{y}{L_y}\right),\\
B_z &= 0.0,\\
\psi &= 0,
\end{aligned}
$$

where $\rho_0 = 1.0$, $L_x = 4$, $L_y = 1$, $\delta = 0.2$, and $\delta_B = 10^{-3}$. In order to sustain the initial current sheet, and allow the instability growth, the following source term is added to the induction equation for B_x

$$\frac{-2}{S}\frac{\sinh(y/\delta)}{\delta^2\cosh^3(y/\delta)}.$$

The effectiveness of the VMS stabilization for low Mach number flows is assessed for the case of $S = 10^4$. In this test, no discontinuity capturing included, only the terms in (5). Fig. 3 shows the density profile along $x = 2$ for the original VMS and the VMS incompressible limit stabilized formulations. It can be clearly observed that the introduced term is able to control the oscillations that were present in the original formulation in this limit.

The magnetic island growth is visualized in Fig. 1 where the temporal evolution of the current magnitude is depicted. Fig. 2 shows the momentum evolution, which increases with the instability growth.

A convergence study has been performed to assess that the implementation achieves the formal order of accuracy. To this end, a reference solution has been computed using a Cartesian grid with 1000×500 elements. The time step has been kept smaller than required, $\Delta t = 10^{-2}$ to avoid error pollution from the time discretization. The problem is evolved to $t = 5$, and the error is presented for the momentum field which has largest error and the slowest rate of convergence at this time, since this is the only field with zero initial conditions that evolves on this timescale. Therefore, the error/convergence rate results solely from the approximation error and does not include the projection error from the initial conditions into the FE space. The meshes used are Cartesian grids with $N_x \times N_x/2$ elements, for $N_x \in \{60, 80, 100, 120, 160\}$. Fig. 4 depicts the $L^2(\Omega)$ error as a function of the number of elements in the x direction. It is observed that second order convergence is recovered in the asymptotic regime.

The overall dissipative characteristic of the scheme is assessed by computing the instability growth rates, ω, for different Lundquist numbers, and compared against results present in the literature. The growth rate is computed

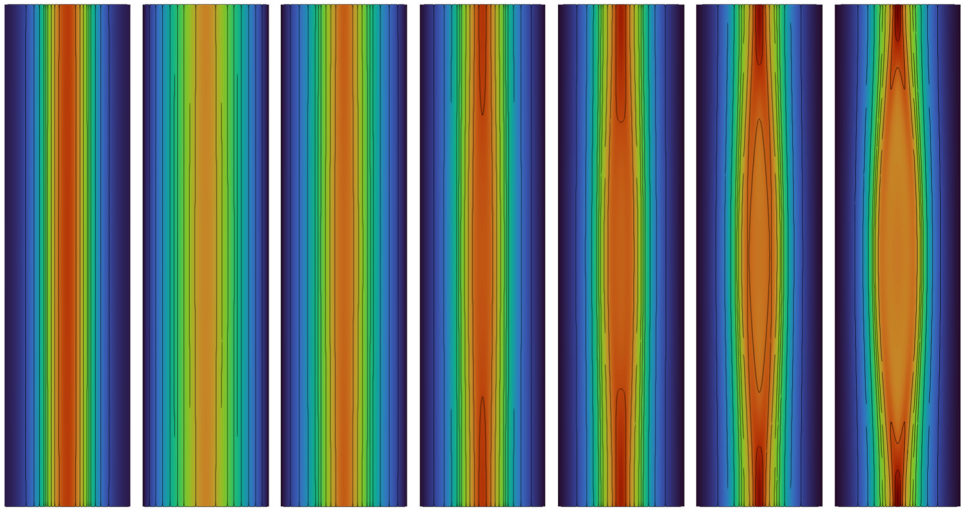

Fig. 1. Current magnitude evolution for $t = \{0, 50, 100, 200, 300, 400, 500\}\tau_A$ (from left to right).

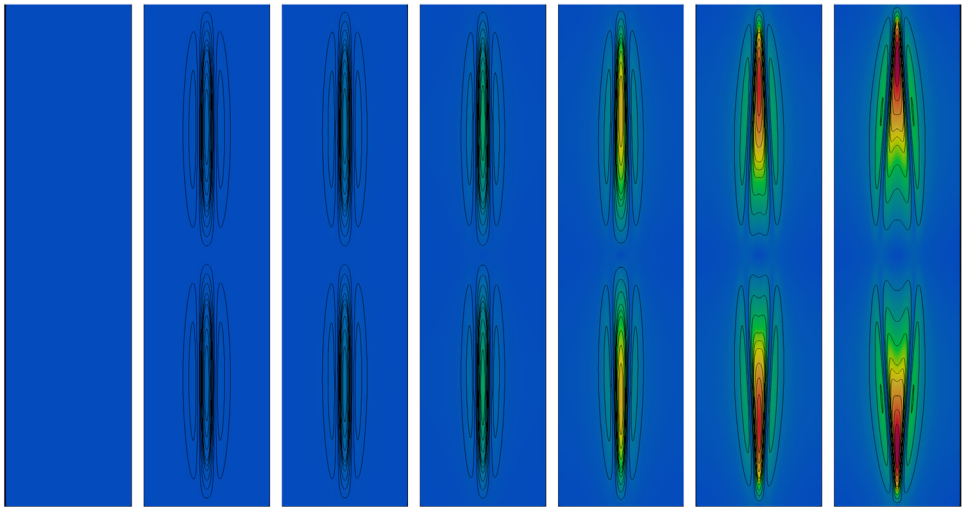

Fig. 2. Momentum magnitude evolution for $t = \{0, 50, 100, 200, 300, 400, 500\}\tau_A$ (from left to right).

using the expression $\|\mathbf{m}\| = C\exp(\omega t)$. Initially, the growth rate shows a nonlinear behavior, followed by a linear phase where ω is constant until it reaches a saturation phase. Fig. 5 depicts the computed growth rates for different Lundquist numbers. In addition, the growth rates using the incompressible formulation from [5], and the results [1] are included for comparison. Excellent agreement is observed between the three results.

5.2. Vertical displacement event (VDE)

In this example, a VDE simulation is performed. Even though the dynamics of the problem are 2D, we solve it in a 3D domain with ITER's reactor geometry. Apart from the plasma, the simulated region also includes a homogenized representation of the first wall and blankets, and the outer vacuum vessel structure. The numerical study is intended to assess the solver scalability, and efficiency for longer timescale simulations.

A VDE occurs if the plasma experiences a change in its equilibrium property that is too fast for the vertical stability control coil to respond. On ITER, this would occur if the plasma suffers a thermal quench, which is a sudden cooling of the plasma at the beginning of a major disruption. The initial vertical displacement can be thought

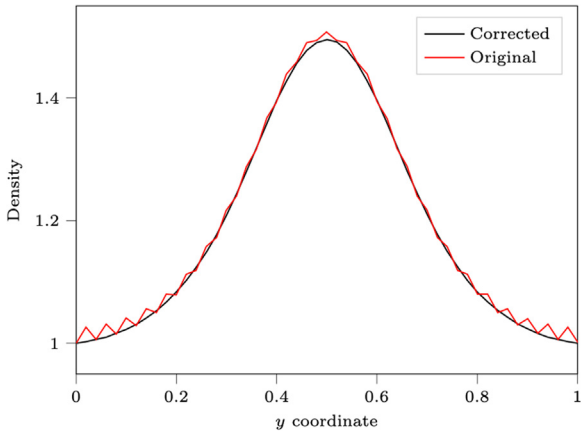

Fig. 3. Density profile at time $t = 31\tau_A$, at $x = 0$, for the solution with and without low Mach number incompressible limit saddle point stabilization.

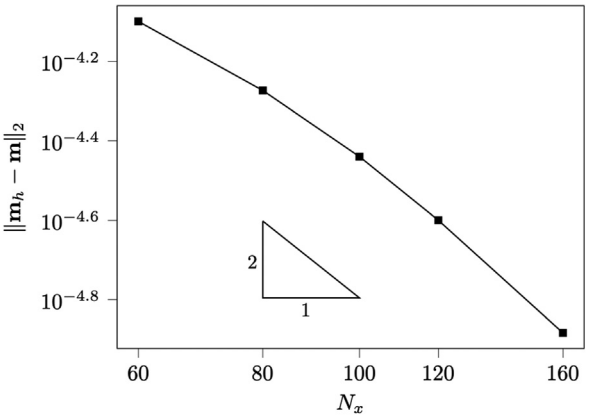

Fig. 4. Convergence rate of the momentum L_2 error for the 2D tearing mode.

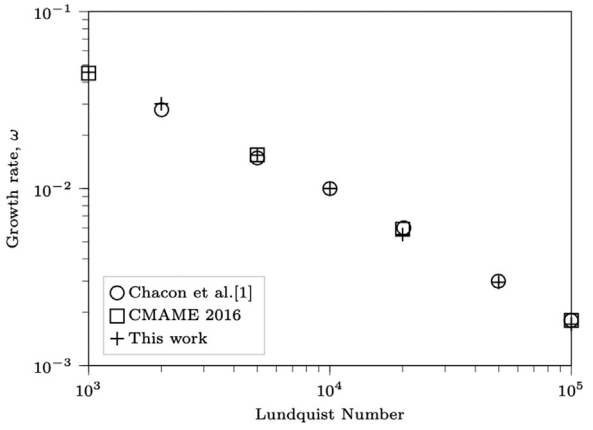

Fig. 5. Growth rate, ω, as a function of the Lundquist number.

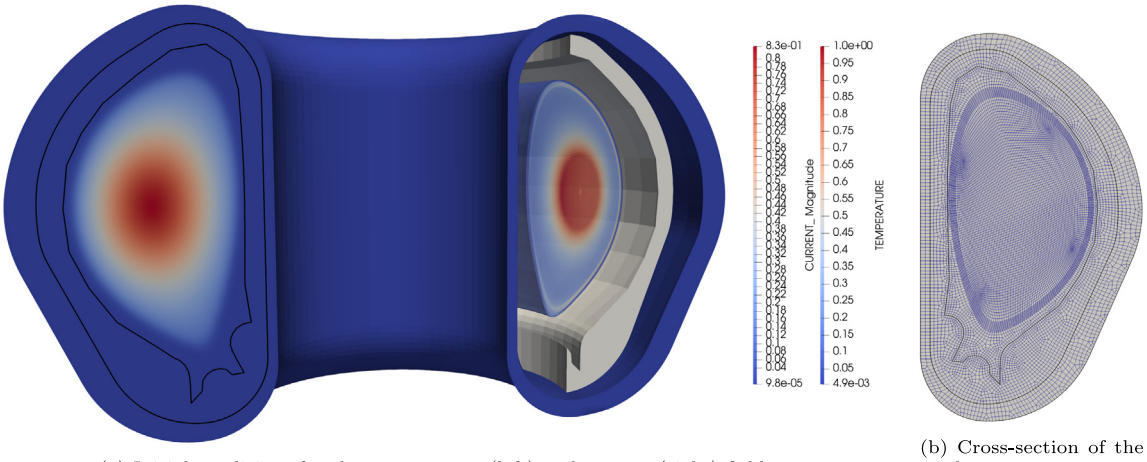

(a) Initial conditions for the temperature (left) and current (right) fields.

(b) Cross-section of the mesh.

Fig. 6. Simulation set-up for a VDE test case.

of as the result of plasma re-establishing force balance, which would approximately satisfy $\mathbf{j} \times \mathbf{B} = 0$. Further vertical displacement of the current-carrying plasma column follows as the cooled plasma resistively dissipates the plasma current. This loss of the vertical positioning control would eventually lead to the current-carrying plasma to scrape off against the chamber wall and thus terminates the plasma discharge in what is called a current quench. If the plasma is sufficiently cold so the Ohmic electric field $\mathbf{E} = \eta\mathbf{j}$ is stronger than the avalanche threshold field, runaway electrons can be efficiently generated for an Ohmic-to-runaway current conversion. However, this effect is not included in the current simulation. In this test, a thermal quench due to radiative cooling is approximated by an artificially increased perpendicular thermal conductivity.

Fig. 6 shows the configuration of the different sub-domain regions, the initial conditions, and the FE mesh used. For the scalability test only the first wall/blanket is considered and the outer domain (vacuum vessel) is considered perfectly conducting. A Reynolds number of 10^3, an isotropic heat conductivity $\kappa = 10^{-3}$, and two different Lundquist numbers are considered, 10^4 and 10^7. The Lundquist number in the wall is set to 10^2. The initial MHD equilibrium has been computed using a Grad–Shafranov solver [58], details of the equilibrium set-up can be found in [58, Sec. 6.2].

Excellent strong scalability results are reported in Fig. 7 for both Lundquist numbers. Fig. 7(c) shows the number of linear iterations per nonlinear iteration remains almost constant, indicating that the strong scaling degradation is an effect of the increased communications and not a degradation of the solver itself.

Fig. 8 shows the results of a weak scaling test for 10^7 Lundquist numbers. The initial mesh contains 347K elements. Two uniform refinements are performed, i.e, at each refinement, each cell is divided in 8 cells. The new nodes are located the centroid of the coarser entities: the midpoint of the coarse edges, the centroid of the coarse faces, and the centroid of the coarse volume. The refined meshes contain 2.77M and 22.2M elements, respectively. The CFL number is kept fixed as the mesh is refined. The results show excellent weak scaling properties, both as a function of time per time step and for the number of iterations.

Fig. 9 shows the temporal evolution of a VDE in the geometry depicted in Fig. 6. For this test a temperature dependent resistivity has been considered for the plasma, resulting in a Lundquist number ranging from 10^7 in the core to 10^4 in the edge for the initial temperature field. The Lundquist number in the first wall is set to 10^4 and to 10^5 in the vacuum vessel. The boundary of the domain is considered perfectly conducting. An anisotropic thermal conductivity with $\kappa_{||} = 0.1$ and $\kappa_{\perp} = 10^{-3}$ has been used.

5.3. (1,1)-Mode internal kink

Finally, a test with a 3D instability in ITER geometry is performed. To this end, a (1,1)-mode internal kink is simulated [59]. Since this is an internal instability, we will ignore the coupling with the wall, so only the plasma

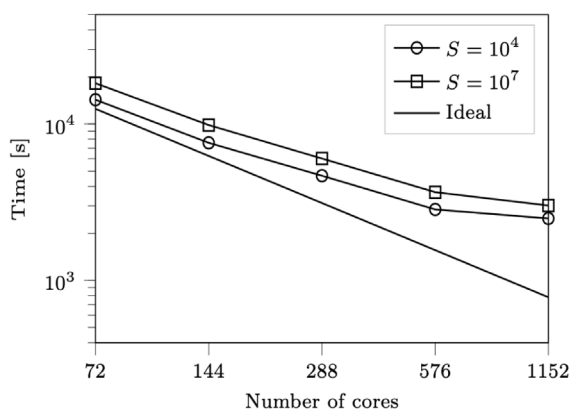

(a) Total run time per number of processors.

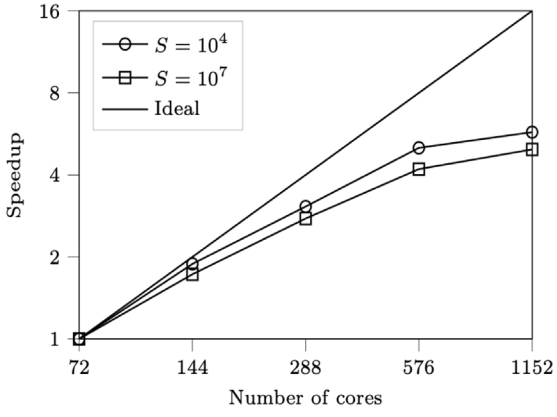

(b) Speedup.

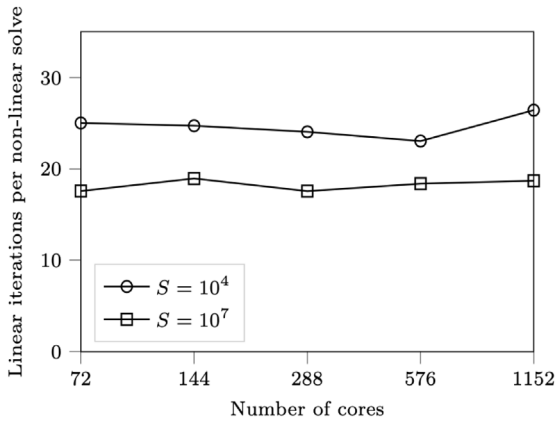

(c) Average linear iterations per nonlinear iteration.

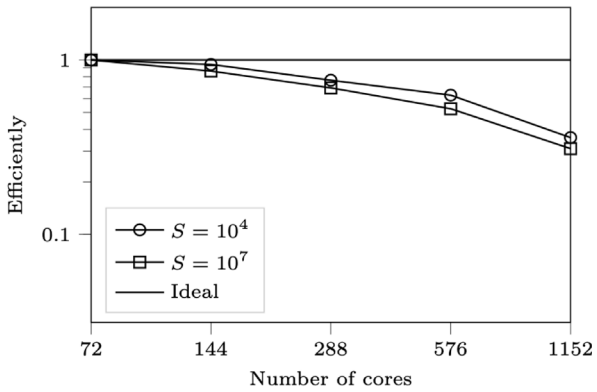

(d) Solver efficiency.

Fig. 7. Scaling results for VDE test for Lundquist numbers $S = 10^4$ and $S = 10^7$.

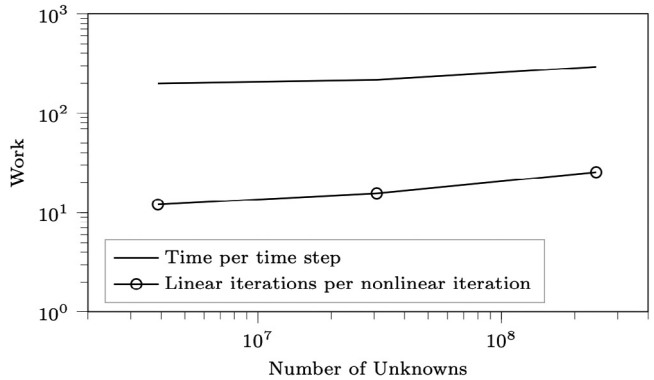

Fig. 8. Weak scaling for VDE test for $S = 10^7$.

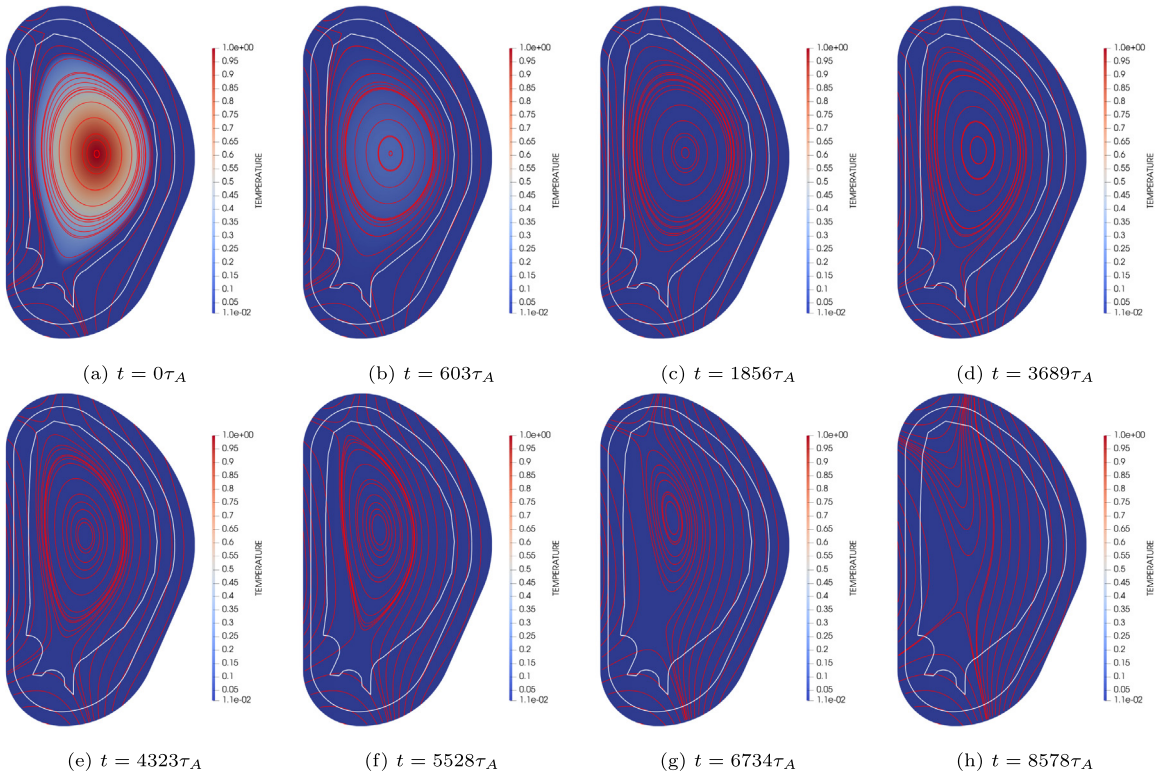

(a) $t = 0\tau_A$ (b) $t = 603\tau_A$ (c) $t = 1856\tau_A$ (d) $t = 3689\tau_A$

(e) $t = 4323\tau_A$ (f) $t = 5528\tau_A$ (g) $t = 6734\tau_A$ (h) $t = 8578\tau_A$

Fig. 9. Evolution of the magnetic field and the temperature during a VDE.

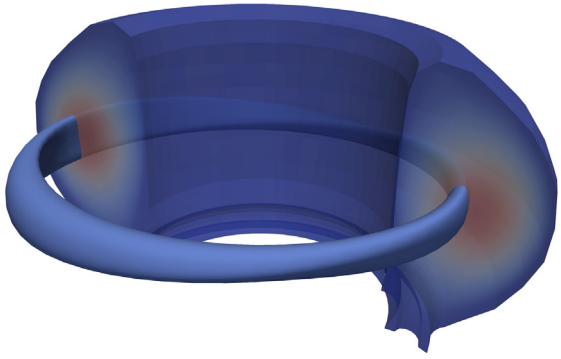

Fig. 10. 3D visualization of an isosurface of the extracted $n = 1$ pressure perturbation included in the initial conditions.

region is considered, as opposed to the previous case where both wall domains where included. The initial conditions are a modification of the previous equilibrium, such that it is highly unstable with respect to the (1,1)-mode (see Fig. 11). In addition, a perturbation of the equilibrium is included to seed the n = 1 mode and trigger the instability growth. Fig. 10 shows the perturbation with a pressure isosurface.

The parameters used for this test are the following. A Reynolds number of 10^5, a temperature dependent resistivity is considered, which Lundquist number ranges from 10^4 to 10^6 for the initial temperature field. The thermal conductivity is set to $\kappa_{||} = 10^{-3}$, and $\kappa_{\perp} = 10^{-5}$. Even though the parameters are modest when compared with realistic physical values, this selection allows for an initial assessment of the formulation to capture complex 3D instabilities. A mesh with 770 240 elements have been used, a cross-section is depicted in Fig. 12. An adaptive time

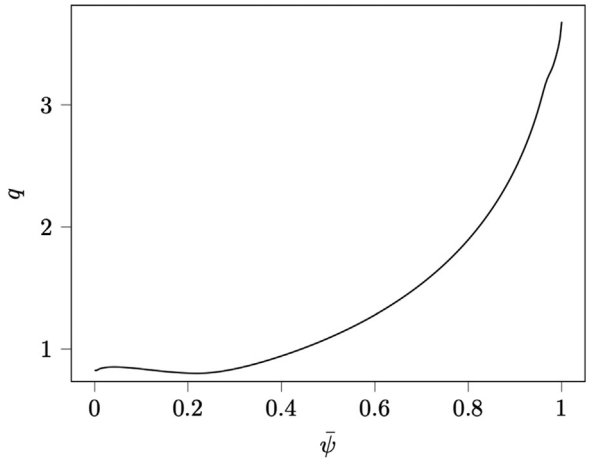

Fig. 11. Safety factor, q, profile as a function of the normalized $\bar{\psi}$ for the initial conditions.

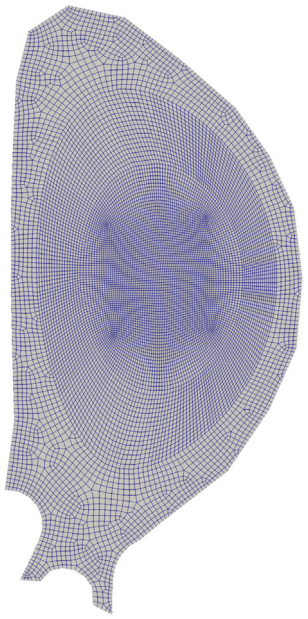

Fig. 12. Cross-section of the mesh used for the (1,1)-mode internal kink simulation.

step has been used, such that the fluid CFL less than 1, $\|\mathbf{u}\|\Delta t/h < 1$, and also bounded by $\Delta t < 2\tau_A$. This leads to a $\Delta t \approx 1.3\tau_A$ for most of the simulation.

To analyze the magnetic field structure a set of Poincaré plots are depicted. To obtain them, a continuum magnetic field is computed via the Hermite interpolation in [60] that preserves the solenoidal property analytically [61]. Fig. 13 shows the time evolution of the magnetic field. A small island can be observed in 13(a), which grows until it becomes the magnetic axis after a saw-tooth crash (see 13(a)–13(d)). This in turn, excites higher m-number modes leading to a disruption-inducing globally stochastic magnetic fields (see 13(h)).

6. Conclusions

A novel VMS formulation for low Mach number compressible visco-resistive MHD flows has been developed. The VMS stabilization is intended to handle highly convected flows with unresolved gradients as well as the saddle

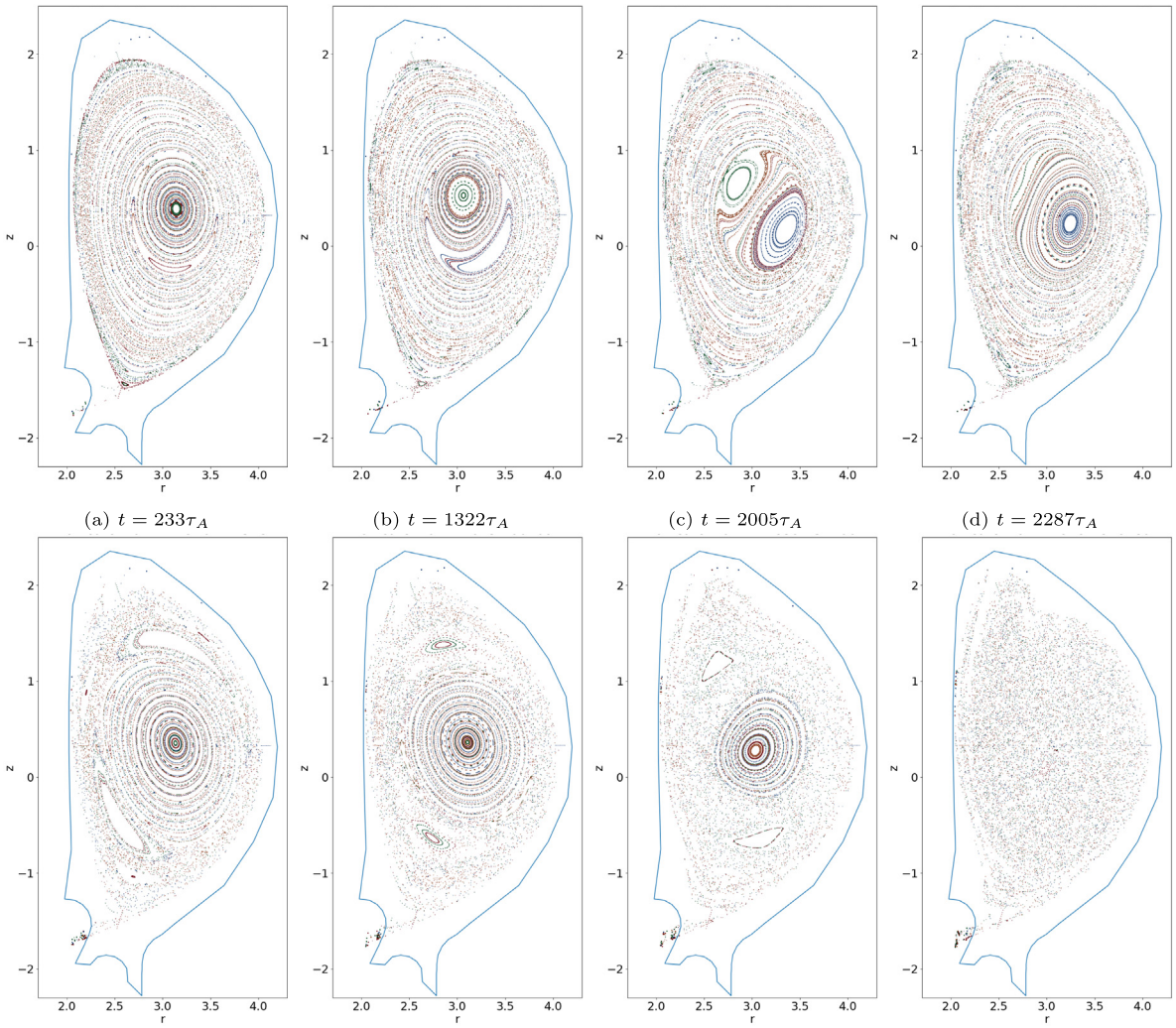

Fig. 13. Poincaré plots for the time evolution of the magnetic field for a 1,1-mode internal kink instability.

point problem generated from introduction of a Lagrange multiplier for enforcing the solenoidal involution on the magnetic field. Additionally a special treatment for stabilizing the saddle point problem arising for the limit of a nearly incompressible flow has been demonstrated. To efficiently handle the multiple-time-scale aspect of fusion plasma formulations and simulations a fully-implicit formulation is presented with preconditioning using an approximate block factorization approach. The numerical experiments show that spurious oscillations triggered by an almost incompressible behavior are effectively controlled with the proposed formulation. Further, the scheme is able to reproduce literature results for the growth rates of a 2D tearing mode, showing it is minimally dissipative. The scheme shows excellent strong and weak scaling properties and also robustness with respect to higher Lundquist numbers (see [53] for an in-depth study). This has enabled the possibility of efficiently performing larger timescale simulations. Additionally, the presented formulation gives flexibility not present in the state-of-the-art codes used for MCF [18,19], both for arbitrary geometry and parallelization. It also enables the usage of highly-scalable block preconditioning strategies. As opposed to other codes using different discretization techniques in (r, z) and ϕ directions to reduce the number of unknowns, but that can lead to restrictions in parallel partitioning techniques and preconditioning strategies. The numerical results in the present work show that adopting the described formulation with the choice of the preconditioner results in a strategy that can lead to efficient large-scale solvers for MCF for

arbitrary geometries. Initial results for a cold VDE and a (1,1) kink-mode show promising results for performing relevant simulations for MCF devices.

Overall, these initial results indicate a that the scheme is robust, scalable, and efficient for challenging visco-resistive MHD problems arising in the simulation of MCF devices. This work enables the exploration of future simulations with more physically realistic models for resistivity and heat conductivity.

Declaration of competing interest

The authors declare that they have no known competing financial interests or personal relationships that could have appeared to influence the work reported in this paper.

Data availability

The authors do not have permission to share data.

References

[1] L. Chacón, D.A. Knoll, J.M. Finn, An implicit nonlinear reduced resistive MHD solver, J. Comput. Phys. 178 (2002) 15–36.
[2] A. Kritz, D. Keyes, Fusion simulation project workshop report, J. Fusion Energy 28 (2009) 1–59.
[3] D.E. Keyes, D.R. Reynolds, C.S. Woodward, Implicit solvers for large-scale nonlinear problems, J. Phys. Conf. Ser. 46 (1) (2006) 433.
[4] J.N. Shadid, R.P. Pawlowski, J.W. Banks, L. Chacón, P.T. Lin, R.S. Tuminaro, Towards a scalable fully-implicit fully-coupled resistive MHD formulation with stabilized FE methods, J. Comput. Phys. 229 (20) (2010) 7649–7671.
[5] J.N. Shadid, R.P. Pawlowski, E.C. Cyr, R.S. Tuminaro, L. Chacon, P.D. Weber, Scalable implicit incompressible resistive MHD with stabilized FE and Fully-coupled Newton-Krylov-AMG, Comput. Methods Appl. Mech. Engrg. 304 (2016) 1–25.
[6] L. Chacón, An optimal, parallel, fully implicit Newton–Krylov solver for three-dimensional viscoresistive magnetohydrodynamics, Phys. Plasmas 15 (5) (2008) 056103.
[7] S.C. Jardin, Review of implicit methods for the magnetohydrodynamic description of magnetically confined plasmas, J. Comput. Phys. 231 (3) (2012) 822–838.
[8] E. Nardon, A. Fil, M. Hoelzl, G. Huijsmans, et al., Progress in understanding disruptions triggered by massive gas injection via 3D non-linear MHD modelling with JOREK, Plasma Phys. Control. Fusion 59 (1) (2016) 014006.
[9] B. Nkonga, J. Tarcisio-Costa, J. Vides, VMS Finite Element for MHD and Reduced-MHD in Tokamak Plasmas, Inria Sophia Antipolis; Université de Nice-Sophia Antipolis, 2016.
[10] J. Kates-Harbeck, A. Svyatkovskiy, W. Tang, Predicting disruptive instabilities in controlled fusion plasmas through deep learning, Nature 568 (7753) (2019) 526–531.
[11] M. Lehnen, K. Aleynikova, P. Aleynikov, D. Campbell, P. Drewelow, N. Eidietis, Y. Gasparyan, R. Granetz, Y. Gribov, N. Hartmann, et al., Disruptions in ITER and strategies for their control and mitigation, J. Nucl. Mater. 463 (2015) 39–48.
[12] P. De Vries, G. Pautasso, D. Humphreys, M. Lehnen, S. Maruyama, J. Snipes, A. Vergara, L. Zabeo, Requirements for triggering the ITER disruption mitigation system, Fusion Sci. Technol. 69 (2) (2016) 471–484.
[13] N.B. Salah, A. Soulaimani, W.G. Habashi, M. Fortin, A conservative stabilized finite element method for the magento-hydrodyanamics equations, Int. J. Numer. Methods Fluids 29 (1999) 535–554.
[14] R. Codina, N. Hernández-Silva, Approximation of the thermally coupled MHD problem using a stabilized finite element method, J. Comput. Phys. 230 (2011) 1281–1303.
[15] R. Codina, N. Hernández-Silva, Stabilized finite element approximation of the stationary magento-hydrodyanamics equations, Comput. Mech. 38 (2006) 344–355.
[16] S. Badia, R. Planas, J.V. Gutiérrez-Santacreu, Unconditionally stable operator splitting algorithms for the incompressible magnetohydrodynamics system discretized by a stabilized finite element formulation based on projections, Internat. J. Numer. Methods Engrg. 93 (3) (2013) 302–328, http://dx.doi.org/10.1002/NME.4392.
[17] S. Badia, R. Codina, R. Planas, On an unconditionally convergent stabilized finite element approximation of resistive magnetohydrodynamics, J. Comput. Phys. 234 (1) (2013) 399–416, http://dx.doi.org/10.1016/J.JCP.2012.09.031.
[18] C.R. Sovinec, A. Glasser, T. Gianakon, D. Barnes, R. Nebel, S. Kruger, D. Schnack, S. Plimpton, A. Tarditi, M. Chu, et al., Nonlinear magnetohydrodynamics simulation using high-order finite elements, J. Comput. Phys. 195 (1) (2004) 355–386.
[19] M. Hoelzl, G.T. Huijsmans, S.J. Pamela, M. Bécoulet, E. Nardon, F.J. Artola, B. Nkonga, C.V. Atanasiu, V. Bandaru, A. Bhole, D. Bonfiglio, A. Cathey, O. Czarny, A. Dvornova, T. Fehér, A. Fil, E. Franck, S. Futatani, M. Gruca, H. Guillard, J.W. Haverkort, I. Holod, D. Hu, S.K. Kim, S.Q. Korving, L. Kos, I. Krebs, L. Kripner, G. Latu, F. Liu, P. Merkel, D. Meshcheriakov, V. Mitterauer, S. Mochalskyy, J.A. Morales, R. Nies, N. Nikulsin, F. Orain, J. Pratt, R. Ramasamy, P. Ramet, C. Reux, K. S rkim ki, N. Schwarz, P. Singh Verma, S.F. Smith, C. Sommariva, E. Strumberger, D.C. Van Vugt, M. Verbeek, E. Westerhof, F. Wieschollek, J. Zielinski, The JOREK non-linear extended MHD code and applications to large-scale instabilities and their control in magnetically confined fusion plasmas, Nucl. Fusion 61 (6) (2021) 065001.
[20] H.R. Strauss, Nonlinear, three-dimensional magnetohydrodynamics of noncircular tokamaks, Phys. Fluids 19 (1) (1976) 134–140.
[21] J.F. Drake, T.M. Antonsen Jr., Nonlinear reduced fluid equations for toroidal plasmas, Phys. Fluids 27 (4) (1984) 898–908.
[22] R. Hazeltine, M. Kotschenreuther, P. Morrison, A four-field model for tokamak plasma dynamics, Phys. Fluids 28 (8) (1985) 2466–2477.

[23] X. Zeng, G. Scovazzi, A variational multiscale finite element method for monolithic ALE computations of shock hydrodynamics using nodal elements, J. Comput. Phys. 315 (2016) 577–608.
[24] J.N. Shadid, E.C. Cyr, R.P. Pawlowski, T.W. Wildey, E. Phillips, D. Hensinger, S. Conde, K. Fischer, A. Robinson, W. Rider, et al., Towards an IMEX Monolithic ALE Method with Integrated UQ for Multiphysics Shock-Hydro, Tech. Rep., Sandia National Lab.(SNL-NM), Albuquerque, NM (United States); Duke Univ ..., 2016.
[25] P. Helander, D.J. Sigmar, Collisional Transport in Magnetized Plasmas, first ed., Cambridge University Press, 2005.
[26] S.I. Braginskii, Transport processes in a plasma, Rev. Plasma Phys. 1 (1965) 205–311.
[27] A. Dedner, F. Kemm, D. Kröner, C.D. Munz, T. Schnitzer, M. Wesenberg, Hyperbolic divergence cleaning for the MHD equations, J. Comput. Phys. 175 (2) (2002) 645–673, http://dx.doi.org/10.1006/jcph.2001.6961.
[28] G. Tóth, The $\nabla \cdot B = 0$ constraint in shock-capturing magnetohydrodynamics codes, J. Comput. Phys. 161 (2) (2000) 605–652, http://dx.doi.org/10.1006/JCPH.2000.6519.
[29] L. Chacón, A non-staggered, conservative, $\nabla \cdot B \to 0$, finite-volume scheme for 3D implicit extended magnetohydrodynamics in curvilinear geometries, Comput. Phys. Comm. 163 (3) (2004) 143–171, http://dx.doi.org/10.1016/j.cpc.2004.08.005.
[30] L. Chacón, D. Del-Castillo-Negrete, C.D. Hauck, An asymptotic-preserving semi-Lagrangian algorithm for the time-dependent anisotropic heat transport equation, J. Comput. Phys. 272 (2014) 719–746.
[31] D. Hu, E. Nardon, M. Lehnen, G. Huijsmans, D. van Vugt, 3D non-linear MHD simulation of the MHD response and density increase as a result of shattered pellet injection, Nucl. Fusion 58 (12) (2018) 126025.
[32] A. Fil, E. Nardon, M. Hoelzl, G.T. Huijsmans, F. Orain, M. Becoulet, P. Beyer, G. Dif-Pradalier, R. Guirlet, H.R. Koslowski, M. Lehnen, J. Morales, S. Pamela, C. Passeron, C. Reux, F. Saint-Laurent, Three-dimensional non-linear magnetohydrodynamic modeling of massive gas injection triggered disruptions in JET, Phys. Plasmas 22 (6) (2015).
[33] N. Ferraro, B. Lyons, C. Kim, Y. Liu, S. Jardin, 3D two-temperature magnetohydrodynamic modeling of fast thermal quenches due to injected impurities in tokamaks, Nucl. Fusion 59 (1) (2019) 016001.
[34] B.C. Lyons, C.C. Kim, Y.Q. Liu, N.M. Ferraro, S.C. Jardin, J. McClenaghan, P.B. Parks, L.L. Lao, Axisymmetric benchmarks of impurity dynamics in extended-magnetohydrodynamic simulations, Plasma Phys. Control. Fusion 61 (6) (2019) 064001.
[35] T. Hughes, Multiscale phenomena: Green's functions, the Dirichlet-to-Neumann formulation, subgrid scale models, bubbles and the origins of stabilized methods, Comput. Methods Appl. Mech. Engrg. 127 (1995) 387–401.
[36] T. Hughes, G. Feijoo, L. Mazzei, J. Quincy, The variational multiscale method: A paradigm for computational mechanics, Comput. Methods Appl. Mech. Engrg. 166 (1998) 3–24.
[37] T.J.R. Hughes, G. Scovazzi, L.P. Franca, Chapter 2: Multiscale and Stabilized Methods in Encyclopedia of Computational Mechanics, Edited By Erwin Stein, Rene de Borst and Thomas J.R. Hughes. Volume 3: Fluids, John Wiley, 2007.
[38] G.A. Wimmer, B.S. Southworth, T.J. Gregory, X. Tang, A fast algebraic multigrid solver and accurate discretization for highly anisotropic heat flux I: open field lines, 2023, arXiv preprint arXiv:2301.13351.
[39] S. Günter, K. Lackner, C. Tichmann, Finite element and higher order difference formulations for modelling heat transport in magnetised plasmas, J. Comput. Phys. 226 (2) (2007) 2306–2316, http://dx.doi.org/10.1016/J.JCP.2007.07.016.
[40] D. Green, X. Hu, J. Lore, L. Mu, M.L. Stowell, An efficient high-order numerical solver for diffusion equations with strong anisotropy, Comput. Phys. Comm. 276 (2022) 108333, http://dx.doi.org/10.1016/J.CPC.2022.108333.
[41] R. Codina, S. Badia, J. Baiges, J. Principe, Variational multiscale methods in computational fluid dynamics, Encycl. Comput. Mech. Second Ed. (2017) 1–28.
[42] T.J. Hughes, G.R. Feijóo, L. Mazzei, J.B. Quincy, The variational multiscale method—a paradigm for computational mechanics, Comput. Methods Appl. Mech. Engrg. 166 (1–2) (1998) 3–24, http://dx.doi.org/10.1016/S0045-7825(98)00079-6.
[43] R. Codina, On stabilized finite element methods for linear systems of convection-diffusion-reaction equations, Comput. Methods Appl. Mech. Engrg. 188 (2000) 61–88.
[44] T. Tezduyar, Stabilized finite element formulations for incompressible flow computations, Adv. App. Mech. 28 (1992) 1.
[45] J.L. Guermond, R. Pasquetti, B. Popov, Entropy viscosity method for nonlinear conservation laws, J. Comput. Phys. 230 (11) (2011) 4248–4267.
[46] T.J. Barth, Numerical Methods for Gasdynamic Systems on Unstructured Meshes, in: Lecture Notes in Computational Science and Engineering, (no. 5) 1999, pp. 195–285.
[47] J.E. Dennis Jr., R.B. Schnabel, Numerical Methods for Unconstrained Optimization and Nonlinear Equations, in: Series in Automatic Computation, Prentice-Hall, Englewood Cliffs, NJ, 1983.
[48] S.C. Eisenstat, H.F. Walker, Choosing the forcing terms in an inexact Newton method, SIAM J. Sci. Comput. 17 (1996) 16–32.
[49] J. Shadid, A fully-coupled Newton-Krylov solution method for parallel unstructured finite element fluid flow, heat and mass transfer simulations, Int. J. CFD 12 (1999) 199–211.
[50] E.C. Cyr, J.N. Shadid, R.S. Tuminaro, R.P. Pawlowski, L. Chacón, A new approximate block factorization preconditioner for 2D incompressible (reduced) resistive MHD, SISC 35 (2013) B701–B730.
[51] E.C. Cyr, J.N. Shadid, R.S. Tuminaro, Teko: A block preconditioning capability with concrete applications in Navier-Stokes and MHD, SIAM J. Sci. Comput. 38 (5) (2016) S307–S331.
[52] P.T. Lin, J.N. Shadid, J.J. Hu, R.P. Pawlowski, E.C. Cyr, Performance of fully-coupled algebaric multigrid preconditioners for large-scale VMS resistive MHD, J. Comput. Appl. Math. 344 (2018) 782–793.
[53] P. Ohm, J. Bonilla, E.G. Phillips, J.N. Shadid, M. Crockatt, R. Tuminaro, J. Hu, X. Tang, Scalable multiphysics block preconditioning for low mach number compressible resistive MHD with application to MCF, 2023 Submitted.
[54] M. Gee, C. Siefert, J. Hu, R. Tuminaro, M. Sala, ML 5.0 Smoothed Aggregation User's Guide, Tech. Rep. SAND2006-2649, Sandia National Laboratories, Albuquerque NM, 87185, 2006.

[55] M.F. Murphy, G.H. Golub, A.J. Wathen, A note on preconditioning for indefinite linear systems, SIAM J. Sci. Comput. 21 (2000) 1969–1972.
[56] H. Elman, V.E. Howle, J.N. Shadid, R. Shuttleworth, R.S. Tuminaro, A taxonomy of parallel mulit-level block preconditioners for the incompressible Navier-Stokes equations, JCP 227 (2008) 1790–1808.
[57] L. Berger-Vergiat, C.A. Glusa, J.J. Hu, M. Mayr, A. Prokopenko, C.M. Siefert, R.S. Tuminaro, T.A. Wiesner, MueLu User's Guide, Tech. Rep. SAND2019-0537, Sandia National Laboratories, 2019.
[58] S. Liu, Q. Tang, X.-z. Tang, A parallel cut-cell algorithm for the free-boundary Grad–Shafranov problem, SIAM J. Sci. Comput. 43 (6) (2021) B1198–B1225, http://dx.doi.org/10.1137/20M1385470.
[59] B.B. Kadomtsev, Disruptive instability in tokamaks, Sov. Tech. Phys. Lett. (Engl. Transl.); (United States) 1:5 (1975) URL https://www.osti.gov/biblio/7147025.
[60] O. Beznosov, D. Appelö, Hermite-discontinuous Galerkin overset grid methods for the scalar wave equation, Commun. Appl. Math. Comput. Sci. 3 (3) (2021) 391–418.
[61] J.M. Finn, L. Chacón, Volume preserving integrators for solenoidal fields on a grid, Phys. Plasmas 12 (5) (2005) 054503.